Ufuk Genç

A Master's Thesis

AGU 2023

ADAPTIVE ONLINE TORQUE SHARING FUNCTION TO MITIGATE TORQUE RIPPLE IN SWITCHED RELUCTANCE MOTORS

A THESIS
SUBMITTED TO THE DEPARTMENT OF ELECTRICAL AND COMPUTER ENGINEERING
AND THE GRADUATE SCHOOL OF ENGINEERING AND SCIENCE OF ABDULLAH GUL UNIVERSITY
IN PARTIAL FULFILLMENT OF THE REQUIREMENTS
FOR THE DEGREE OF
MASTER OF SCIENCE

By
Ufuk Genç
May 2023

ADAPTIVE ONLINE TORQUE SHARING FUNCTION TO MITIGATE TORQUE RIPPLE IN SWITCHED RELUCTANCE MOTORS

A THESIS
SUBMITTED TO THE DEPARTMENT OF ELECTRICAL AND COMPUTER ENGINEERING
AND THE GRADUATE SCHOOL OF ENGINEERING AND SCIENCE OF ABDULLAH GUL UNIVERSITY
IN PARTIAL FULFILLMENT OF THE REQUIREMENTS
FOR THE DEGREE OF
MASTER OF SCIENCE

By

Ufuk Genç

May 2023

SCIENTIFIC ETHICS COMPLIANCE

I hereby declare that all information in this document has been obtained in accordance with academic rules and ethical conduct. I also declare that, as required by these rules and conduct, I have fully cited and referenced all materials and results that are not original to this work.

Name-Surname: Ufuk Genç

Signature :

REGULATORY COMPLIANCE

M.Sc. thesis title Adaptive Online Torque Sharing Function to Mitigate Torque Ripple in Switched Reluctance Motors has been prepared in accordance with the Thesis Writing Guidelines of the Abdullah Gül University, Graduate School of Engineering & Science.

Prepared By	Advisor
Ufuk Genç	Asst. Prof. Burak Tekgün
Signature	Signature

Head of the Electrical and Computer Engineering Program

Assoc. Prof. Zafer Aydın

Signature

ACCEPTANCE AND APPROVAL

M.Sc. thesis title Adaptive Online Torque Sharing Function to Mitigate Torque Ripple in Switched Reluctance Motors and prepared by Ufuk Genç has been accepted by the jury in the Electrical and Computer Engineering Graduate Program at Abdullah Gül University, Graduate School of Engineering & Science.

05 /05/2023

(Thesis Defense Exam Date)

JURY:

Advisor : Asst. Prof. Dr. Burak Tekgün…….....

Member : Prof. Dr. İrfan Alan…….....

Member : Asst. Prof. Dr. Yusuf Yaşa…… .....

APPROVAL:

The acceptance of this M.Sc. thesis has been approved by the decision of the Abdullah Gül University, Graduate School of Engineering & Science, Executive Board dated ….. /….. / …….. and numbered ……..……. .

…….. /…….. / ……..
(Date)
Graduate School Dean
Prof. Dr. İrfan ALAN

ABSTRACT

ADAPTIVE ONLINE TORQUE SHARING FUNCTION TO MITIGATE TORQUE RIPPLE IN SWITCHED RELUCTANCE MOTORS

Ufuk Genç
MSc. in Electrical and Computer Engineering
Advisor: Asst. Prof. Burak Tekgün

May 2023

Electrical machines play a crucial role in modern society by transforming electrical energy into mechanical energy and vice versa. These machines include various types of motors and generators, which are used in a wide range of applications such as electric vehicles, industrial automation, and renewable energy systems. One of the popular electrical machines is the switched reluctance machine (SRM), which is known for its high reliability and efficiency. The key advantages of the SRM include its simple structure, robustness, and low cost. The SRM does not require a permanent magnet or an excitation winding, making it an attractive option for high-volume, low-cost applications. Despite its advantages, the SRM also has some disadvantages that need to be considered. One of the main drawbacks of the SRM is being susceptible to torque ripple, which can result in vibration and noise. In order to overcome these disadvantages, advanced control methods have been developed for the SRM. One such control method is the torque sharing function, which distributes the load among the phases of the motor. This results in improved torque characteristics and reduced torque ripple. However, this control method also has some disadvantages, such as increased complexity and the need for more advanced sensors and controllers. Additionally, the torque sharing function may result in reduced efficiency, especially at high speeds. The purpose of this thesis study is to improve the torque ripple performance of SRM for a wide speed range through the proposed control approach.

In conclusion, minimizing the torque ripple is a critical aspect of the operation of SRMs, and a range of control strategies and techniques can be used to achieve this goal. By reducing the torque ripple, SRMs can deliver improved efficiency, performance, and reliability, making them even more attractive for a wide range of applications.

Keywords: Switched reluctance machine, instantaneous torque error compensation, adaptive torque sharing, torque ripple minimization.

ÖZET
ANAHTARLAMALI RELÜKTANS MOTORLARINDA TORK DALGALANMASININ AZALTILMASI İÇİN UYARLANABİLİR ÇEVRİMİÇİ TORK PAYLAŞIM FONKSİYONU GELİŞTİRİLMESİ

Ufuk Genç
Elektrik ve Bilgisayar Mühendisliği Anabilim Dalı Yüksek Lisans
Tez Yöneticisi: Dr. Öğretim Üyesi Burak Tekgün

Mayıs 2023

Elektrik makineleri, elektrik enerjisini mekanik enerjiye ve tersine dönüştürerek toplumda kritik bir rol oynar. Bu makineler, elektrikli araçlar, otomasyon ve yenilenebilir enerji sistemleri gibi geniş bir uygulama yelpazesinde kullanılan çeşitli motor ve jeneratör tiplerini içerir. Yüksek güvenilirlik, sağlamlık ve düşük maliyet nedeniyle, anahtarlamalı relüktans motoru popüler bir elektrik motorudur. Bu motorlar, kalıcı mıknatıs ve rotorunda herhangi bir sargı içermez ve bu, yüksek hacim ve düşük maliyet gerektiren uygulamalarda bu tür motorların tercih edilmesine neden olur. Ancak, avantajlarına rağmen, bu motorların bazı dezavantajları vardır. Bu dezavantajların başında tork dalgalanması gelir ve bu da motorda titreşime ve gürültüye neden olur. Bu sorunu azaltmak için geliştirilmiş tork kontrol yöntemleri uygulanır. Tork paylaşım fonksiyonu yöntemi, motor fazlarında torku eşit şekilde dağıtarak motorun tork kontrolünü gerçekleştirir. Fazlar arasında torkun eşit şekilde dağıtılması, daha iyi tork karakteristikleri ve azaltılmış tork dalgalanması sağlar. Ancak, bu kontrol yöntemi de bazı dezavantajlara sahiptir, örneğin artan karmaşıklık ve daha gelişmiş sensörler ve kontrolörler gerektirir. Ayrıca, tork paylaşım fonksiyonu özellikle yüksek hızlarda düşük verimliliğe ve tork dalgalanmasına neden olabilir. Bu tez çalışmasının amacı, önerilen bir kontrol yaklaşımıyla SRM'nin yüksek hızlı uygulamalarda tork dalgalanması performansını iyileştirmektir. Tork dalgalanmasının azaltılması, anahtarlamalı relüktans motorlarının verimliliği, performansı ve güvenilirliğini arttırarak, çeşitli kontrol stratejileri ve teknikleri kullanılmasıyla mümkündür. Bu hedefe ulaşmak, motorların geniş bir uygulama yelpazesinde daha çekici hale gelmesini sağlar.

Anahtar Kelimeler: Anahtarlamalı Relüktans Motoru, Tork hata kompansatörü, adaptif tork paylaşımı, tork dalgalanması azaltılması

Acknowledgments

I would like to express my gratitude to my advisor, Dr. Burak Tekgün, for his guidance, encouragement, and support during my graduate studies. His technical knowledge, process management, and human qualities have illuminated me throughout this process.

I would like to thank The Scientific and Technological Research Council of Türkiye (TUBİTAK) for supporting my graduate studies under 2210-D Domestic industry-focused master's scholarship program.

I'm so grateful to my colleagues in the AGÜ Power Laboratory for their continuous assistance and for providing the best educational work environment and for the good times that we had together while working.

Finally, and most importantly, I would like to thank my family and friends for their continuous help and support at all times.

TABLE OF CONTENTS

LIST OF FIGURES

LIST OF TABLES

LIST OF ABBREVIATIONS

AC	Alternative Current
W'	Co-Energy
DC	Direct Current
DITC	Direct Instantaneous Torque Control
DTC	Direct Torque Control
ER	Energy Conversion Ratio
FEA	Finite Element Analysis
GA	Genetic Algorithm
LPF	Low-Pass Filter
LUT	Look-Up Table
W	Magnetic Energy
MCU	Micro Controller Unit
SRM	Switched Reluctance Motor
TSF	Torque Sharing Function

To my parents…

Chapter 1

Introduction

Electrical machines are being increasingly used in order to create a more environmentally friendly world and reduce energy consumption. The most popular types of electrical machines are induction and permanent magnet synchronous machines, which have advantages such as efficiency and high-speed capability. However, due to the copper windings in the rotor or the use of permanent magnets, the interest in these machines is shifting in another direction as the use of electrical machines increases over time. To address this concern, researchers have focused on developing simpler and more environmentally friendly electric motors, such as Switched Reluctance Machines (SRM). Unlike other types of motors, SRMs do not have permanent magnets or wound rotor coils, making them simpler and less expensive to manufacture. However, one of the main challenges with SRMs is the presence of torque ripple [1], which refers to fluctuations in torque output as the rotor rotates. While the design of SRMs can help to reduce torque ripple, this alone may not be enough. Therefore, the control algorithm approach is significantly important, especially in high-speed applications. By improving the control algorithm, it is possible to further reduce torque ripple and improve the performance of SRMs. As such, the development and use of SRMs are becoming increasingly important in the quest for more environmentally friendly and efficient electrical machines.

1.1 Problem Statement and Hypothesis

Research Question: How to perform a control on SRM to mitigate the torque ripple, while maintaining instantaneous torque reference tracking in a simpler way?

Problem Statement: Conventional SRM control methods result in poor torque ripple performance, which makes the SRM less favorable among other machine types. Being one of the first invented electric machines, SRM has various superiorities over other

machine types, like having a simple structure and being cost effective, which makes them a powerful alternative for today's developing electric vehicle market. Torque ripple minimization techniques have been extensively studied over the years, one of which is the torque sharing function technique. This technique is widely researched due to its effectiveness in reducing torque ripple and has been implemented in various applications. However, at higher speeds, it becomes challenging to track the reference current with the actual current, which leads to a ripple in high-speed applications. Additionally, adapting the controller to the speed variations is a challenge where it can reduce efficiency.

Hypothesis: Adaptive torque sharing function approach based on the instantaneous torque estimations is a strong alternative to the conventional Torque Sharing Function (TSF) because the consecutive phases of the SRM have different inductance characteristics, allowing them to be controlled differently based on their unique characteristics. This method can improve torque ripple performance from low-speed to high-speed applications and reduce peak current in the incoming phase, which helps to reduce copper losses. Additionally, this technique can prevent the occurrence of negative torque, improving both the performance of the motor and the reliability of its components.

1.2 Research Objectives and Motivation

The reduction of carbon footprint and energy consumption to achieve an environmentally friendly world has become a primary focus of researchers [2]. Electric motors used in industry consume roughly 50% of the world's total electricity [3], making the development of more efficient and power-saving motors crucial. These result in a growing interest in electric motor design and control with advancements in semiconductor technologies and fast processing programs. Permanent magnet synchronous motors (PMSM) have been developed to replace induction and DC motors, but their high cost and susceptibility to heat demagnetization remain as its drawbacks. SRM, on the other hand, has gained attention due to its unique design that eliminates the need for rotor windings and their durability, affordability, and eco-friendliness. SRMs have a fast-dynamic response and small rotor inertia, which make them ideal for precision control applications. However, their operation based on the reluctance principle produces a pulse torque form, causing a lack of a sinusoidal waveform when compared to PMSMs and IMs. The stator current structure of SRMs has a distinctive waveform, known as the

commutation region, in which consecutive phases are active, which adversely affects the motor's iron loss, torque ripple performance, and system efficiency [4], [5]. The torque ripple performance is a crucial parameter, and the studies based on the optimization-based torque-sharing methods can reduce the torque ripple between the consecutive phases according to the literature. Nevertheless, these methods require significant processing power and offline operation, which limits their practicality in real-time applications.

In this study, it is aimed to develop a torque control approach that can operate with a decent torque ripple performance above the base speed with cascaded and adaptive torque control strategies. The proposed control approach prioritizes maximum torque production from the outgoing phase, given its high inductance value, while simultaneously reducing or if possible preventing negative torque generation that could increase torque ripple. The incoming phase current control regulates the total torque in the commutation period based on the estimated torque error by utilizing the incoming phase, which has a low inductance value. Consequently, minimizing torque ripple is a crucial factor in the operation of the SRMs, and there are various control methods available to achieve this objective. By minimizing torque ripple, SRMs can provide better efficiency, performance, and reliability, thereby making them more appealing for a diverse range of applications.

This thesis is presented in five chapters. Chapter 1 gives a brief explanation of the SRMs, their advantages and disadvantages, and the research objectives and motivations of this thesis. Chapter 2 explains the SRM's operation principles, their structure, and motor driver topologies. This chapter also includes motor control strategies. Chapter 3 presents how to model and simulate SRM in a simulation platform. This chapter also includes the simulation results of hysteresis current control and TSF explained in the details in Chapter 2. Chapter 4 takes an in-depth look at the proposed adaptive torque-sharing control strategy. Chapter 5 presents the results and discussion. Chapter 6 recommends future works about the control of the SRM for improving the controller performance and mitigating the torque ripple.

Chapter 2

Literature Review

2.1 Introduction

SRM was first used to move an electric locomotive in the mid-1800s but was not a viable solution in the industry because the motor was too difficult to control and the switching frequency was inefficient at that time. However, innovations such as the invention of the semiconductor, the improvement of the microcontroller (MCU) technology, and the increasing usage of computer aided engineering analysis tools in such motors.

SRM, which does not have a permanent magnet in the rotor compared to the induction and DC motor offers a solution in terms of both environmentally friendly and cost-effective to the consumer. In addition, due to its robustness, it attracts the attention of researchers for the use of SRM from low-speed to ultra-high-speed motors [6].

2.2 Advantages and disadvantages of SRM

Using SRMs has major advantages and disadvantages [7]–[9] for the end-user and manufacturer. These advantages are listed below.

- Since there is no permanent magnet in the rotor, the manufacturing cost is low.
- Due to the fact that the phases are independent of each other and each phase is driven separately, the fault tolerance and ruggedness of the motor are higher compared to AC motors. Therefore, these motors can operate even when a single-phase is lost.
- SRM can operate efficiently at high speeds due to the absence of a winding in the rotor and the small air gap.

- The rotor copper loss cannot be considered in this motor as there is no winding on the rotor, which has an advantage for the cooling system when it comes to thermal evaluation.

The disadvantages are listed below.

- SRM has a double salient construction. Therefore, the torque ripple of the SRM is higher than the other type of motors such as permanent magnet and induction motors.
- The excitation of the phase in a machine can generate radial forces that produce undesired acoustic noise and vibration, which are widely recognized as adverse effects.
- They have a low power factor when operating at low loads. Because SRM operates in the linear region of magnetization at low currents.

2.3 Literature Survey

Over the years, research has shifted its focus towards developing more environmentally friendly methodologies. In this regard, electric motors have emerged as essential tools since they help reduce carbon emissions as compared to internal combustion engines, and are a key enabling technology for promoting an eco-friendlier world. The stator of the SRM is made of double-salient pole copper windings, whereas the rotor also features a double-salient structure devoid of any windings or permanent magnets. Consequently, these motors are both robust and eco-friendly. However, the SRM suffers from a high torque ripple. There are primarily two methods to mitigate this ripple. The first one involves motor optimization where the stator and rotor pole numbers, as well as their respective pole arcs are optimized to mitigate torque ripple [10]. The second approach focusses on motor control. Numerous torque ripple minimization methods are developed, based on firing angle control, various current profiling, and direct and indirect torque control techniques [7].

2.3.1 Optimization of the Firing Angles

The various control methods to reduce torque ripple has been extensively studied in the literature. The commutation period between the consecutive phases is the primary cause of the torque ripple. The firing angles can notably influence the average torque and torque ripple so, the control of its are a well-known strategy to achieve minimum torque ripple in the literature. In [11], the optimization of the firing angles is employed using online measurement and Finite Element Analysis (FEA). In [12], the turn-off angles are determined, and a multi-objective optimization technique is applied to obtain the minimum torque ripple. The motor efficiency is improved with the firing angle controller based on the reference torque and motor position in [13]. However, optimal angles are not enough to minimize the total torque ripple so, the control technique that focusing on for decades by researchers is torque control and various torque control methods have been proposed during the commutation period in the literature. The torque control techniques classified as direct torque control method (DTC), direct instantaneous torque control (DITC), current profiling technique, direct flux control (DFC), and torque sharing function (TSF)

2.3.2 Direct Instantaneous Torque Control

DITC was first introduced in [14] based on torque estimation and chopping control. This control approach is a suitable torque control method till the base speed with the suitable firing angles and allows for four-quadrant operation [15]. The torque ripple is minimized by separately controlling the turn-on and turn-off angles. In [16], while the turn-on angle is determined based on the reference torque and speed, an online optimization technique is used to determine the turn-off angle. [17] proposed a DITC method, which is based on the turn-on and turn-off angle positions, and torque ripple is minimized with the torque error regulator and endpoint detector to stator current. In [18], the turn-on angle is optimized with the reference torque and speed to regulate the torque with DITC in high-speed applications. In [19], torque ripple performance is improved, and the torque ripple-free speed range is extended. In [20], the current control (CC) and DITC control approach are combined to extend the speed range. The phase torque characteristic is separated into four discrete regions called the incoming phase region, the phase excitation region, the current control region, and the demagnetization region, and

the control approach is determined by these angles accordingly. Further explanations are provided for the DITC in Chapter 3.

2.3.3 Direct Torque Control

The DTC strategy obtains a good torque performance in the induction machine and is implemented in [21]. This method is regulated the torque base on the torque error and flux-linkage error and also flux-linkage vector estimation. Conventional DTC methods can generate negative torque by mitigating the torque-ampere ratio. To address this issue, a new DTC method is proposed in [22], which does not require active control of the motor's flux and is designed to reduce negative torque. In this proposed method, the voltage vector and turn-off angle are regulated in real-time to prevent the generation of negative torque. In [23], proposes an alternative torque estimation method that employs sliding mode control and a sliding mode observer, instead of a PI controller. This method is used to estimate the reference torque for the system. In [24], proposes a new method for sensorless rotor location estimation using the DTC method, based on the maximum and minimum inductance points. This method is suitable for low-level industrial applications. However, for high-power applications such as those in the aerospace and military industries, where safety is essential, accurate rotor location estimation is crucial. Therefore, this method may not be suitable for high-power applications. In [25], discusses a new DTC strategy aimed at improving efficiency and torque ripple performance. This method uses a new switching pattern that divides the space-vector structure into 16 sectors and modifies the selection of voltage vectors to eliminate phase current extension into the negative inductance slope region.

2.3.4 Current Profiling Technique

The current profiling method is an effective torque control approach that determines the reference current without the look-up tables (LUT). The study of [26] used the Fourier series to explain the optimal current and introduced an objective function to minimize torque ripple and reduce copper loss. In [27], outlines two methods for minimizing torque ripple. The first method involves designing the SRM to have a symmetric torque characteristic to reduce torque ripple. However, this approach alone may be insufficient to effectively minimize torque ripple. Therefore, a high-performance torque controller is proposed, which uses an initial reference current obtained from an offline method and

adjusts the current based on torque feedback. Also, the current profiling technique used in the learning control algorithm is proposed in the literature. The fuzzy logic is presented to minimize the torque ripple [28] and sensorless position estimation [29] The work of [30], a new method is presented for reducing torque ripple in SRM. This method utilizes a cerebellar model articulation controller (CMAC) neural network. The purpose of the CMAC neural network is to control the switching angles of the motor to reduce the torque ripple.

2.3.5 Torque Sharing Function

The TSF has been commonly preferred and applied in SRM drivers [1]. TSF is a method where reference torque is shared with mathematical expression in the commutation period. The conventional TSFs such as linear, sinusoidal, cubic, and exponential functions in the literature determine the pattern of the consecutive phases. In [31], the conventional TFSs are optimized using the genetic algorithm (GA) to determine optimal turn-on and overlapping angles. Here, the copper loss and torque ripple performance were investigated based on the cost-weighting factor. Finally, the exponential TSF was evaluated as the optimal method with respect to torque ripple performance. In [32], the ant colony algorithm is used to determine the optimum firing angles of the cubic TSF. The turn off angle and overlapping angle are calculated based on the turn-on angle to mitigate the computational cost. In [33], the offline TSF approach is used employing the Tikhonov factor based on phase currents and their derivatives for mitigating copper loss and the time derivative of flux linkage. In [34], the optimal current profile depending on the voltage of the phase is reported using the static flux linkage characteristics. The torque ripple is observed as 13% at low speed, and it is recorded as 22% at the base speed. In [35] a novel TSF is reported for reducing the torque ripple in between consecutive phases. In [36], torque ripple minimization is achieved using the nonlinear modulation that regulates sequential phases based on the rotor location and outgoing phase current. The phases of regulation include three different methods and selected linear and non-linear functions according to the saturation; thus, the current tracking capability increases. The torque ripple of a four-phase SRM at base speed is given as 8%. In [37], a dynamic control model of the SRM that has better current tracking performance is introduced and the generated negative torque at the end of the commutation is compensated with the incoming phase. Though the torque ripple is

mitigated in the dynamic control method, the incoming phase current is increased as compensation for the negative torque that occurs end of the commutation, which results in a higher copper loss. At the rated speed, the torque ripple of this method is given as 28%. In [38], the flux-linkage controller is reported as non-linear TSF. Saturation in the system considers regulating the commutation period. In [39], the non-linear logical TSF that has the switching period adjusted with the torque error is employed to regulate sequential phases. Here, the incoming phase is selected for the main torque generation and the outgoing phase is regulated according to the incoming phase. But the incoming phase has a low inductance profile so the generated torque cannot generate sufficient torque at the high-speed application, which causes an increase in the torque ripple. In [40] two subregions during the commutation period are determined based on the absolute flux-linkage variation for consecutive phases. The SRM can operate at high speeds. In [41], the current control technique which has a two-operation mode introduced in [39] is developed by using an online TSF that the parameters are obtained with the optimization.

2.4 Conclusion

This chapter provides a brief history of SRMs, including their development over time and major milestones in their evolution. Additionally, it explores the advantages and disadvantages of using SRMs in various applications. Furthermore, this chapter discusses the various torque control methods proposed in the literature for the reduction of torque ripple, including model-based and learning control algorithms. The effectiveness of these methods is compared, and their limitations and challenges are discussed.

Chapter 3

Principles of SRM Drive: Operation and Control

3.1 Introduction

This chapter provides an overview of the SRM operation principles, common motor drive topologies, and current and torque control techniques.

3.2 Operation Principle

An SRM consists of double salient poles on both the rotor and stator, as shown in Figure 3.1. The stator and rotor cores are made of ferromagnetic material. However, the rotor core does not have any excitation source, whereas the stator core has coils wound around each stator pole.

The design of an SRM can vary based on the number of phases and poles on the rotor and stator. The phase and pole numbers are determined according to the requirements of the SRM being designed. Increasing the number of phases and stator poles decreases the torque ripple of the SRM and provides a better starting torque. However, controlling the phase currents becomes more challenging.

The operation principles of an SRM are based on Ampere's law and electromagnetic forces, similar to other types of electric motors. When a phase is energized, the magnetic flux flows through the air gap between the stator and rotor. The resistance to this magnetic flux path in the magnetic circuit is called reluctance (symbolized by $\Re$). The magnetic reluctance is given by:

$$\Re = \frac{l_{ag}}{\mu_0 A_c} + \frac{l_c}{\mu_0 \mu_c A_c} \tag{3.1}$$

This equation considers several factors, such as the length of the flux path in the core (l_c) and the length of the flux path in the air gap (l_{ag}), the cross-sectional area of the flux path (A_c), and the magnetic permeability of both airs (μ_0) and the core (μ_c). As a result, the rotor moves towards the stator pole to achieve the lowest possible reluctance. However, as the rotor moves relative to the energized stator, the air gap distance changes, leading to variations in reluctance and magnetic flux linkage based on the motor's position.

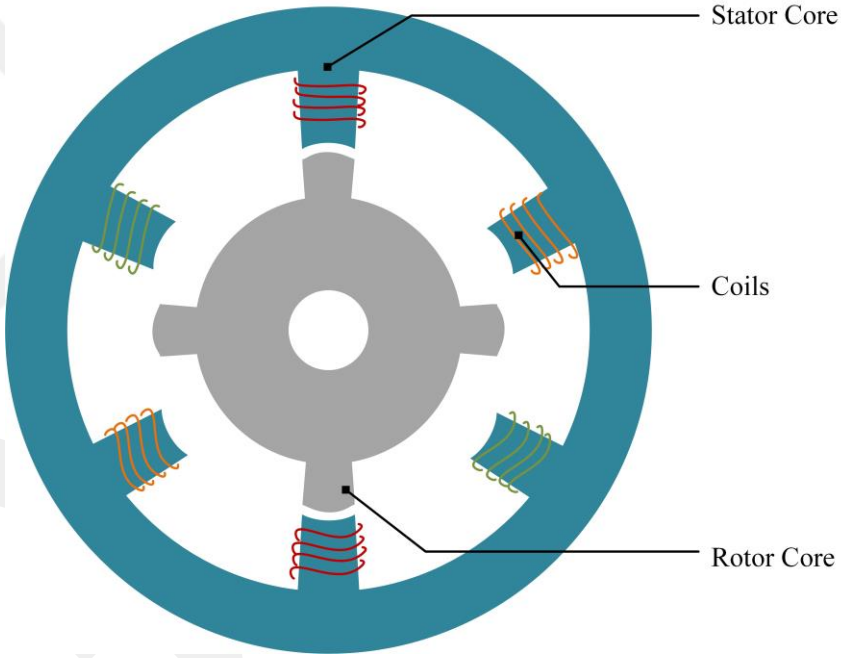

Figure 3. 1 Structure of the SRM.

The minimum reluctance of an SRM, where inductance and flux linkage are at their maximum, is known as the aligned position, where the stator and rotor overlap. The rotor's position situated between the sequential stator poles, which has the minimum inductance and magnetic flux linkage value, is called an unaligned position. The variation of inductance based on the rotor location is shown in Figure 3.2.

The general equation that applies to an individual coil of the SRM is expressed as follows:

$$V_{ph} = i_s r + \frac{d\lambda}{dt} \tag{3.2}$$

In the given equation, *"V_{ph}"* denotes the DC bus voltage in the stator phase, *"i"* represents the instantaneous current flowing through the stator, *"r"* signifies the resistance of the stator winding, and *"λ"* denotes the stator flux linkage. The flux linkage is changed with the position of the rotor and stator current, and it is represented as follows:

$$\lambda = \lambda(i,\ \theta) \tag{3.3}$$

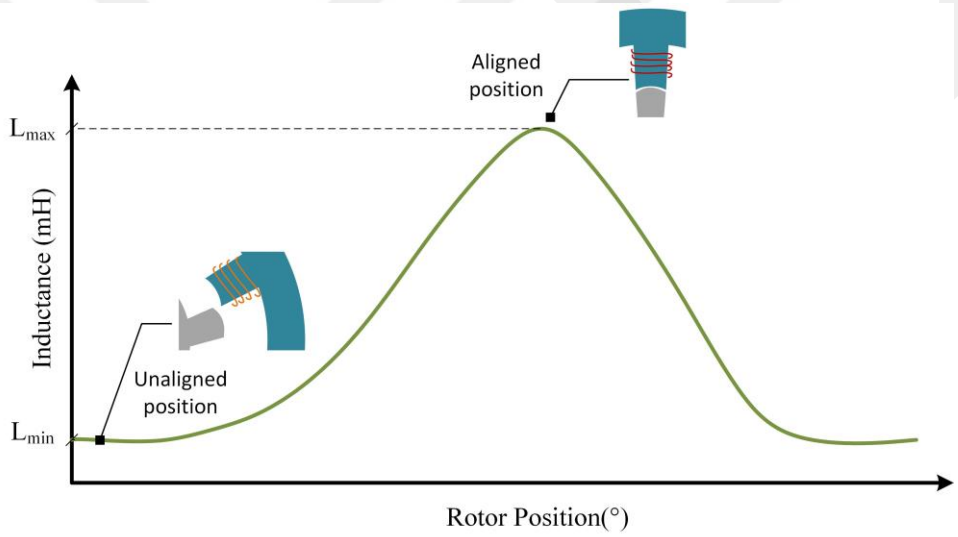

Figure 3. 2 Inductance variation profile in the SRM.

In order to achieve maximum efficiency from the magnetic circuit, the SRM is typically driven with high magnetic saturation. However, this saturation leads to a non-linear relationship between the magnetic field strength and both the rotor location and the stator phase current. Consequently, the mathematical modeling of the SRM becomes more complex.

Assuming magnetic linearity, the flux linkage λ is defined as follows:

$$\lambda = L(\theta, i_s) i_s \tag{3.4}$$

Therefore, it is possible to express the phase voltage equation with the phase inductance and the speed of the SRM as follows:

$$V_{ph} = i_s r + \frac{d\lambda}{dt} = i_s r + \frac{dL(\theta, i_s)i}{dt} = ir + L(\theta, i_s)\frac{di_s}{dt} + i_s \frac{d\theta}{dt}\frac{dL(\theta, i_s)}{d\theta} \tag{3.5}$$

Equation 3.5 comprises three terms that account for the resistive voltage drop, inductive voltage, and back emf voltage in the SRM. Although this equation shares similarities with the voltage equation of a DC motor, the back emf voltage in an SRM is generated differently.

In DC motors, the back-emf voltage is generated by the rotating magnetic field, whereas in an SRM, it is obtained from the instantaneous flux linkage time derivation.

The back emf voltage of the SRM is written by

$$e = i_s \frac{d\theta}{dt}\frac{dL(\theta, i_s)}{d\theta} \tag{3.6}$$

The balance of power relationship can be used using the energy conversion of SRM. The instantaneous power can be written by multiplying both sides with the current in the equation given in Equation 3.5.

$$\begin{aligned} P &= V_{ph} i_s = i_s^2 r + i_s L(\theta, i_s)\frac{di_s}{dt} + i_s^2 \frac{d\theta}{dt}\frac{dL(\theta, i_s)}{d\theta} \\ &= i_s^2 r + (L(\theta) i_s \frac{di_s}{dt} + \frac{1}{2} i_s^2 \frac{dL(\theta, i_s)}{d\theta}\frac{d\theta}{dt}) + \frac{1}{2} i_s^2 \frac{dL(\theta, i_s)}{d\theta}\frac{d\theta}{dt} \\ &= i_s^2 r + \frac{d}{dt}(\frac{1}{2} L i_s^2) + \frac{1}{2} i_s^2 \frac{dL(\theta, i_s)}{d\theta}\omega \end{aligned} \tag{3.7}$$

where, $d\theta/dt$ is called the rotor angular position and represented ω. The first term in Equation. 3.7 is called stator conductor loss, the latter term is the time derivative of magnetic stored energy, and the last term is called mechanical output power. The concept of stored magnetic energy W and co-energy W', as shown in Figure 3.3, can be used to explain the energy conversion process that occurs in SRMs to generate torque.

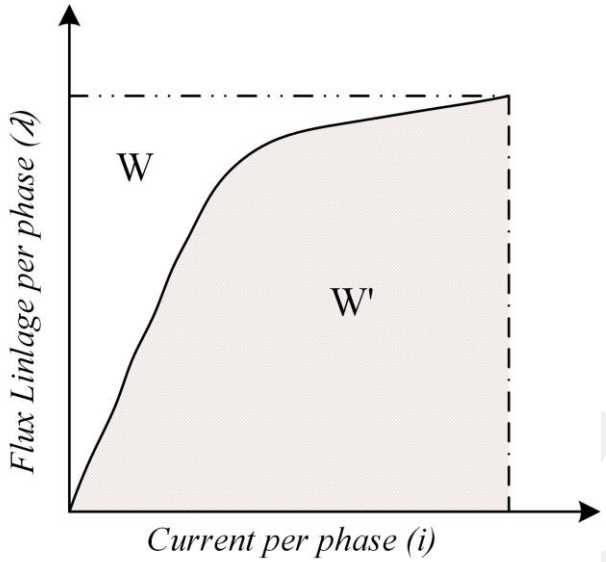

Figure 3. 3 The waveform of the energy conversion in the standby mode.

When a constant current is considered and the stator resistance is ignored, the total electrical energy is equal to the sum of the stored magnetic energy (*W*) and co-energy (*W'*). After the co-energy is converted into mechanical output, the magnetic stored energy can be retrieved as electrical energy. The electrical system can retrieve the stored magnetic energy by using a suitable converter, and it is not lost during the energy conversion process. In SRMs, it is preferable to operate the motor at currents high enough to cause magnetic saturation because this increases energy conversion rates.

The energy conversion ratio (*ER*) is calculated as follows

$$ER = \frac{w}{w + w'} \tag{3.8}$$

In an SRM, the energy *W'* is the energy that is being converted to mechanical work, and *W* is the energy that is sent back to the converter when the rotor moves from the unaligned to the aligned condition as shown in Figure 3.4.

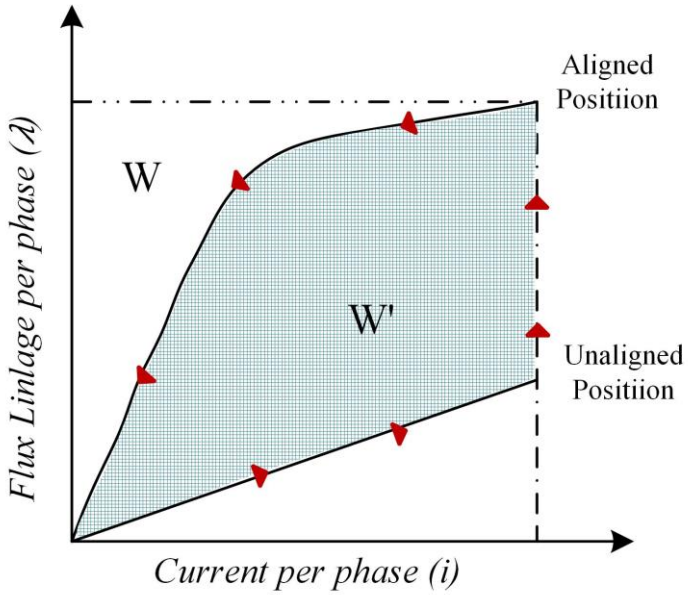

Figure 3. 4 The waveform of the energy conversion in the operation mode.

The torque produced in the SRM depends on the reluctance principle. This reluctance principle means that the SRM always tends to the minimum reluctance air gap. Torque production of the SRM can be represented mathematically as

$$T_{ph} = \frac{\partial W'(\theta, i_s)}{\partial \theta}\Big|_{i_s=\text{constant}} \tag{3.9}$$

The coenergy (W') can be defined as

$$W' = \int \lambda(\theta, i_s)\, di_s = \int L(\theta, i_s)\, i_s\, di_s \tag{3.10}$$

Where the inductance L and the flux linkage λ of the SRM depend on the rotor location and stator current. Thus, the co-energy considered linear magnetic characteristics can be expressed simplified torque production equation.

$$T_{ph} = \frac{dL(\theta, i_s)}{d\theta} \times \frac{i^2}{2} \tag{3.11}$$

In Equation 3.11, the instantaneous generated torque of the SRM is depicted, and the total torque is the summation of the torque produced by each phase. Furthermore, the generated torque is directly proportional to the square of the stator phase current, and its direction isn't dependent on the phase current. The use of unipolar stator current in SRM drivers makes them more economical since a single switch is sufficient to control the

stator current in a phase. Figure 3.5 represents the simplified one-phase excitation. The polarity of the torque production is determined by the time derivative of the inductance value, as per Equation 3.11. Thus, positive torque generation occurs during the ascending inductance slope, while negative torque generation occurs during the descending inductance slope.

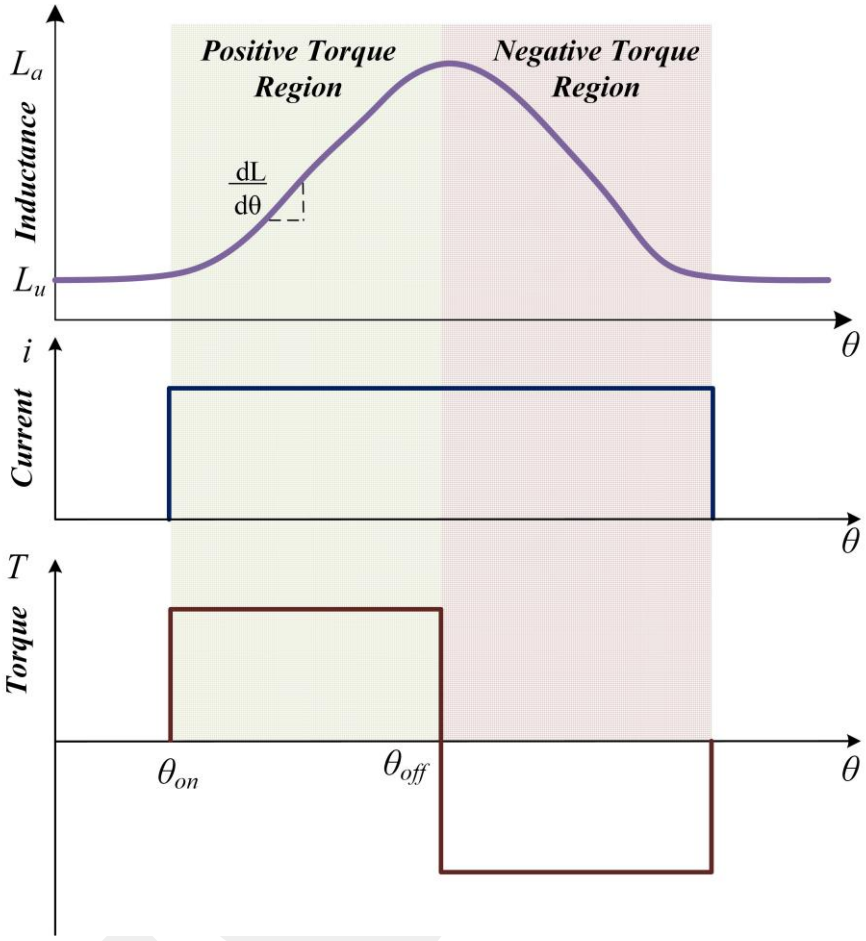

Figure 3. 5 Idealized inductance, current, and torque profile.

3.3 Motor Driver Topologies

The polarity of the SRM torque is independent of the sign of the stator current; hence, the stator current has a unipolar form. This unipolar form enables isolation between the phases. Therefore, the SRM operates fault-tolerantly. SRM can still operate even if there is a phase that has a fault during SRM operation. That's why this leads to the development of many different converter topologies. The selection of the converter to be used depends on the application of the motor and the number of phases.

The asymmetric bridge converter most used converter in the SRM drive as shown in Figure 3.6. The main advantage of this converter, it makes possible independent current control and good torque control. Other advantages of the asymmetric bridge converter are that it is easier to control and provides greater adaptability and is suitable for high-power applications. However, the main disadvantage of this drive is that it includes two switched and two diodes per phase. That's why, it is costly for low-cost applications.

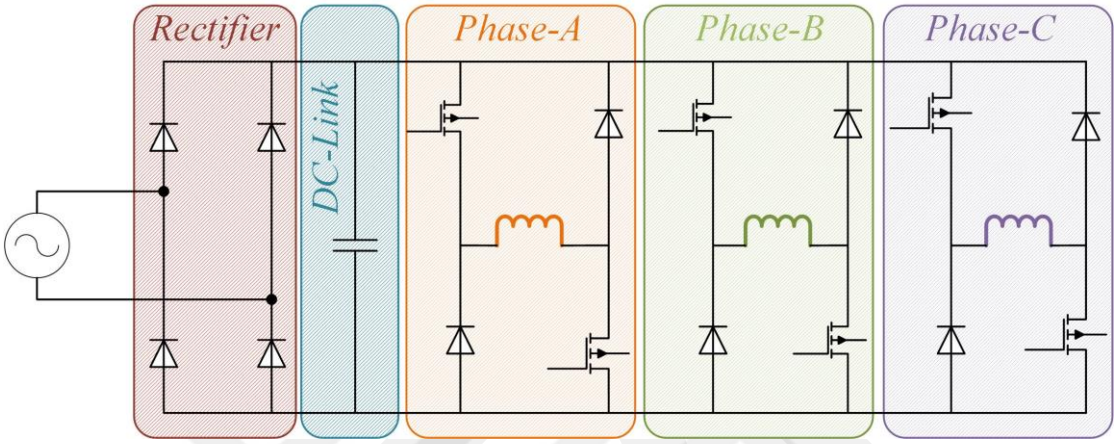

Figure 3. 6 Asymmetric three-phase converter for SRM.

The asymmetric converter operates under three distinct conditions. The first condition is the magnetization mode, which involves turning on both the upper and lower switches. This allows the current to pass through the switches while the diodes remain off. As a result, the stator winding receives the DC bus voltage, which increases the stator current passing through the phase. The second condition is the demagnetization mode, where both switches are turned off. In this case, the diodes are used to return the built-up stator current in the phase windings to the source. This causes the stator current flowing from the diodes to apply a negative DC bus voltage in the stator phase winding, resulting in a sharp reduction in the stator current. Finally, the third condition is the freewheeling mode, where either the lower or upper switch and diode are turned on, causing the stator current to slowly decrease. The freewheeling mode can be further categorized into two separate modes, namely mode 1 and mode 2, which serve the purpose of reducing the switching frequency. All four modes are illustrated in Figure 3.7 for clarity.

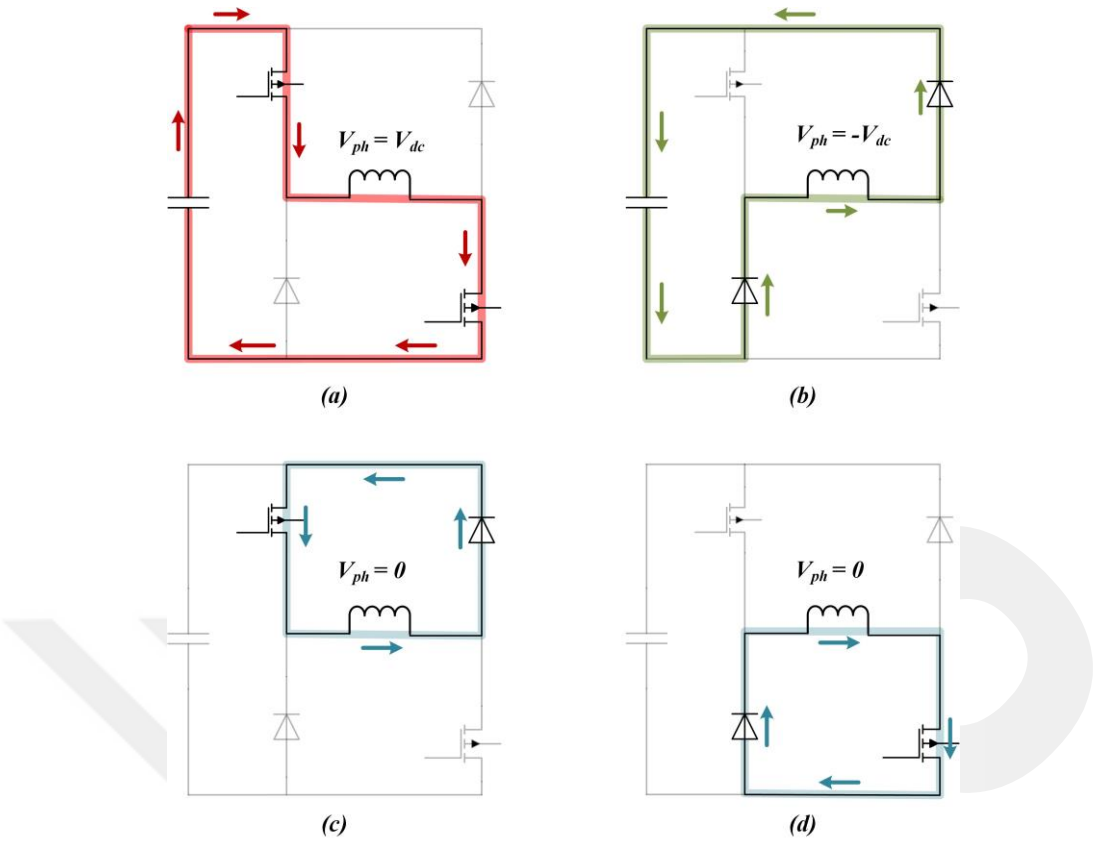

Figure 3. 7 Three modes of Asymmetric Bridge Converter: (a) Magnetization, (b) Demagnetization, (c) Freewheeling Mode 1, (d) Freewheeling Mode 2.

This study compares several converter topologies, including (N+1)-Switched Converters, N-Switched Converters, and C-Dump Converters [42]. The investigation revealed that (N+1)-Switched Converters lead to significant torque ripple since they do not offer independent control of the stator current during commutation. N-Switched converters are further divided into three distinct topologies: bifilar, split dc, and ac converters. Compared to the asymmetric bridge converter, the bifilar converter has higher power device voltage ratings despite having only one control switch for each phase [43]. The dc split converter exhibits higher torque ripple compared to the asymmetric bridge converter and is suitable for low-speed applications [42]. The C-Dump converter and Split AC converter are among the available converter topologies that exhibit similar performance to the asymmetric bridge converter, with lower torque ripple and wider speed range. However, the C-Dump converter's disadvantage is its inefficiency, as the energy stored in the phase is consumed by the resistor when the transistor is turned off [42]**.** Other converter topologies that are detailed in [7], [43] were not examined in this study as the asymmetric bridge converter topology was used.

3.4 Control Techniques

SRMs exhibit torque ripple due to their double salient structure, which can be separated into high-frequency and commutation torque ripple [44]. The commutation torque ripple is the main cause of torque ripple and arises from the region where two phases are active. On the other hand, high-frequency torque ripple occurs during phase current and torque control processes, which vary according to the switching element, control method, and motor parameters. Figure 3.8 shows the total torque waveform for the 24/16 SRM. Numerous control techniques aim to mitigate torque ripple, making SRM control techniques distinct from those of other machines. SRM control techniques can be classified as speed control, torque control, and current control, as shown in Figure 3.9.

The reference speed input commands the torque or stator currents to adjust SRM speed. The speed control unit regulates speed using instantaneous speed information obtained from the encoder. Typically, a PI controller is selected as the speed controller in the SRM. The torque and current control methods are discussed in the following subsections.

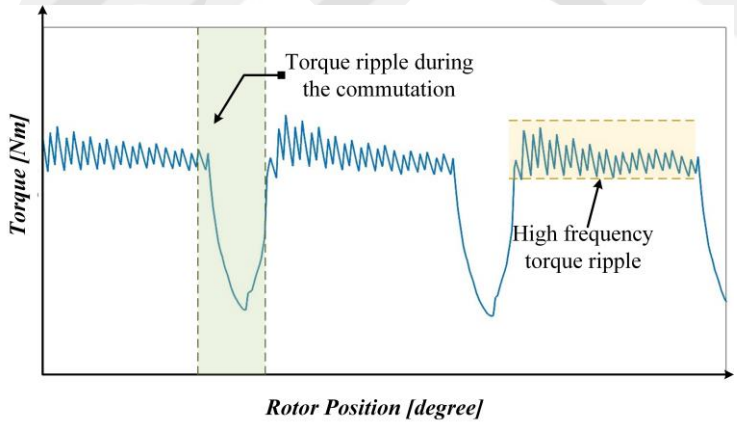

Figure 3. 8 Torque ripple waveform for an 24/16 SRM.

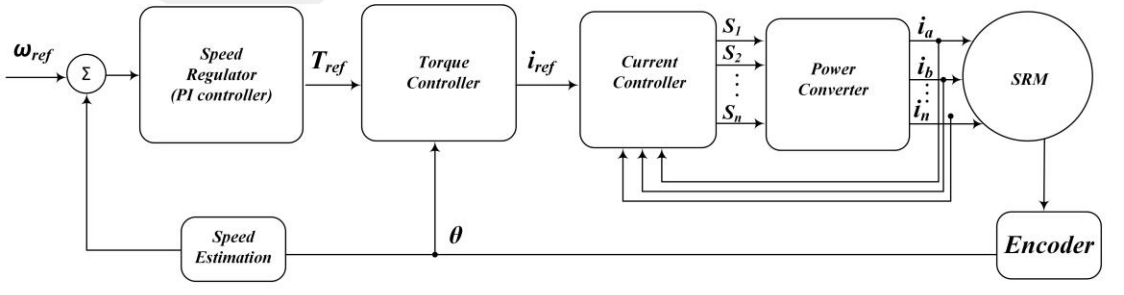

Figure 3. 9 Feedback control scheme for SRM.

3.4.1 Current Control

To ensure the smooth operation of the machine and prevent the stator current from exceeding thermal limitations, it is necessary to control the stator current based on the reference current value obtained from the torque controller. The hysteresis current control method is widely preferred in SRM current control due to its fast-dynamic response and independence from the model [45]. This method involves setting upper and lower limitations that define the hysteresis band. Two methods can be used for controlling the phase current: hard switching and soft switching. With hard switching, the driver operates in magnetization and demagnetization modes, while with soft switching, the driver can operate in magnetization, demagnetization, and freewheeling modes. Although hard switching offers a faster response, it requires a higher switching frequency and results in a higher harmonic phase current. Decreasing the hysteresis band can provide better current tracking performance and mitigate current ripple, resulting in improved torque ripple and acoustic noise performance. Figure 3.10 shows the hysteresis current control and phase voltage. The value at which the phase current is maintained constant is defined by I_{ref}, with I_{max} and I_{min} calculated based on the reference current and hysteresis band, as shown in Equation 3.12. The hysteresis band ($2h$) can be selected according to the switching components, current sensor, and motor control performance.

$$\begin{aligned} I_{\max} &= I_{ref} + h \\ I_{\min} &= I_{ref} - h \end{aligned} \tag{3.12}$$

To maintain the phase current within the hysteresis band, the driver applies positive and negative DC-link voltage, which is monitored through feedback from the current sensor. This method is commonly referred to as hard switching. When the winding current is absent, the driver operates in freewheeling mode to prevent switching losses. Additionally, the inductor of the SRM phase follows a precise mathematical relationship between phase voltage and current, which can be expressed as follows:

$$V_{ph} = L_{ph} \frac{di_{ph}}{dt} \tag{3.13}$$

where, V_{ph}, L_{ph}, and di_{ph}/dt is represented phase voltage, and phase inductance time derivative of current, respectively. As the motor moves from the unaligned position to the

aligned position, the inductance value increases while the time derivative of the current value decreases in accordance with Equation 3.13. Consequently, the switching frequency varies during hysteresis control. It becomes increasingly challenging to control the current as the rotor approaches the aligned position because of the reduced time derivative of the current value. Therefore, as depicted in Figure 3.10, θ_2 is greater than θ_1.

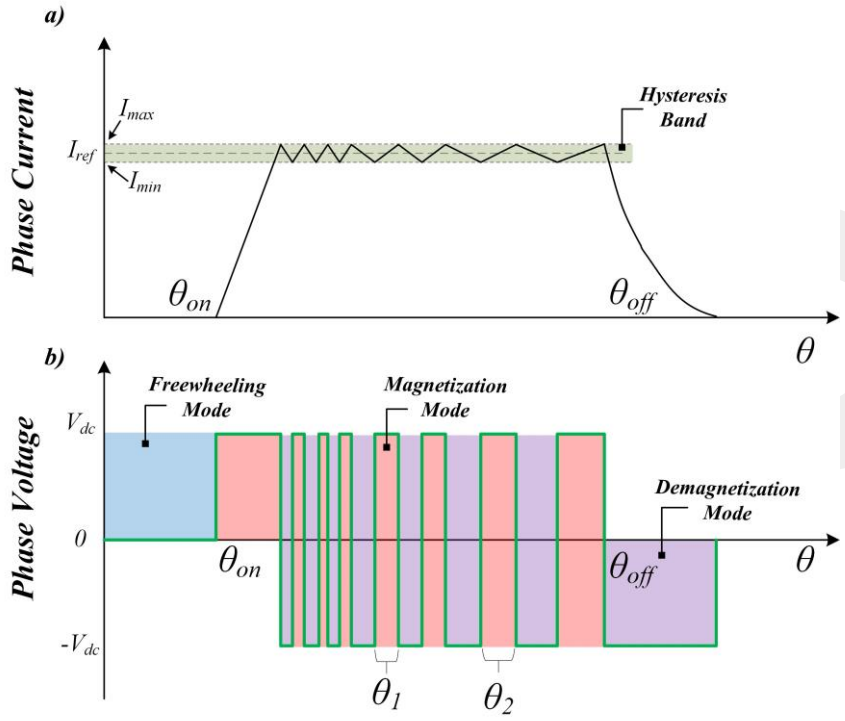

Figure 3. 10 Hysteresis current control for SRM (a) phase current (b) phase voltage.

3.4.2 Torque Control

Torque control in the SRM can be categorized into two methods: direct and indirect, depending on the type of feedback used. In the indirect method, the phase current feedback is utilized to regulate the torque, while in the direct method, the torque is controlled based on the feedback from direct torque estimation.

Direct methods are categorized as direct torque control (DTC) and direct instantaneous torque control (DITC) as shown in Figure 3.11.a and Figure 3.11.b, respectively.

The primary objective of the indirect torque control method is to regulate the torque by controlling the phase current. This method is highly effective because the torque is

directly proportional to the phase current, as shown in Equation 3.10. The indirect torque control method includes several techniques, such as the current profiling technique and the TSF method, as discussed in [44].

3.4.2.1 Direct Instantaneous Torque Control

The DITC method comprises two main components: torque estimation and hysteresis torque control, as shown in Figure 3.11.a The torque error can be obtained by comparing the torque estimation obtained from a LUT with the reference torque. This torque error is then used to generate the appropriate switching signal in the hysteresis control block.

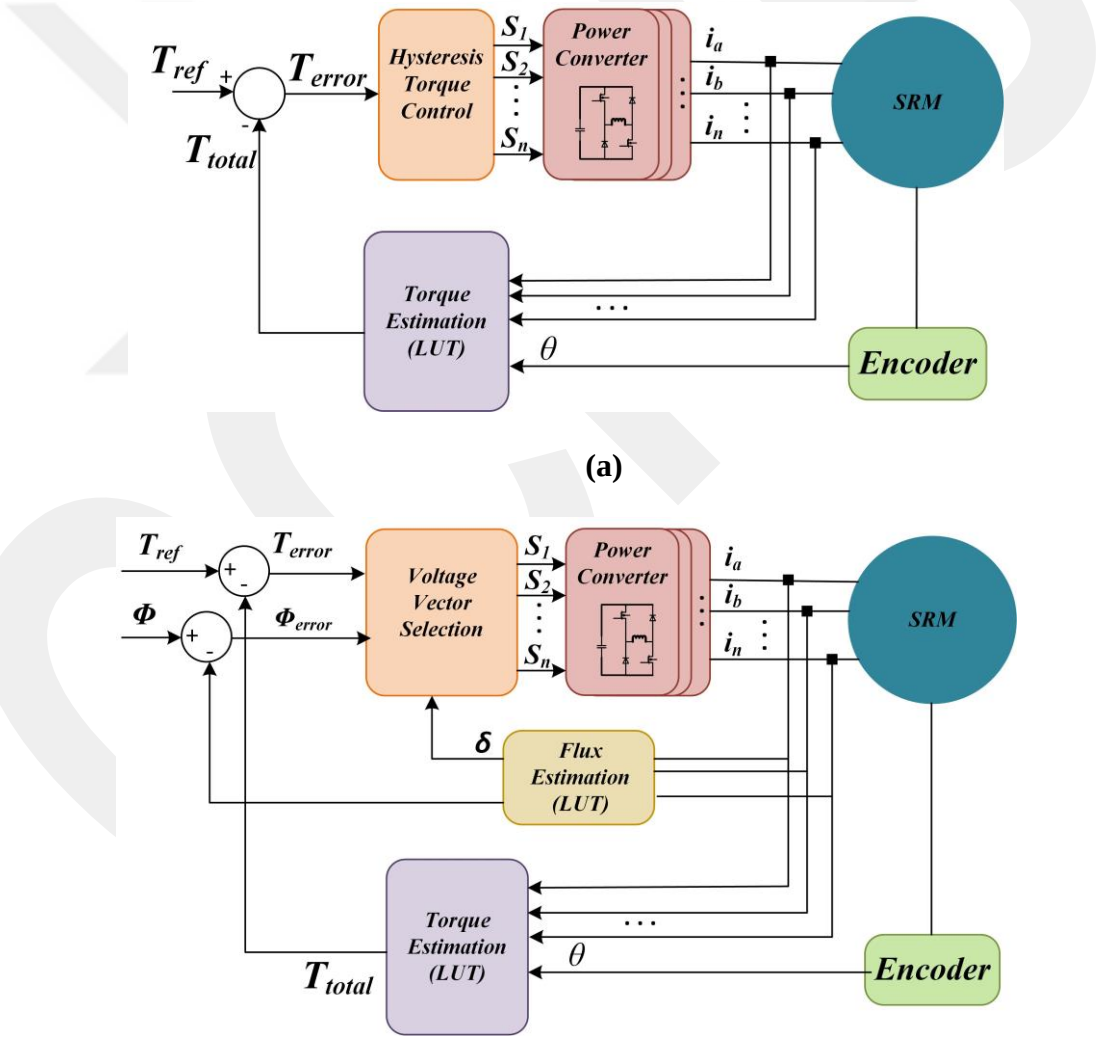

Figure 3. 11 (a) DITC Block Diagram and (b) DTC block diagram.

3.4.2.2 Direct Torque Control

Despite the fact that this method is predominantly used in controlling AC motors, researchers have attempted to utilize this method in SRM to achieve optimal torque performance. The DTC method aims to achieve instantaneous torque regulation by varying the flux linkage while keeping the phase current constant, as depicted in the mathematical expression Equation 3.14.

$$T \cong i_{ph} \frac{\partial \phi}{\partial \theta}, i = \text{constant} \tag{3.14}$$

Fig. 3.11b shows the DTC method. The voltage vector selection is performed to maintain stable torque and flux linkage within a hysteresis band and can be determined based on the torque error, stator flux error, and flux vector feedback (δ).

3.4.2.3 Current Profiling Technique

The current profiling technique involves regulating the reference current with respect to the desired torque performance. This technique is primarily based on the direct definition of the reference current without using an *i(T, θ)* look-up table.

3.4.2.4 Torque Sharing Function

In contrast to the current profiling technique, which directly determines the reference current without using a look-up table, the TSF is a highly effective method that initially separates the reference torque. Compared to other methods, the TSF is a more practical and simple torque control method, as discussed in [7]. Due to the nature of SRMs, the reference torque must be separated from adjacent phases, as torque ripple occurs during the separation of adjacent phases, which is referred to as the commutation period. Figure 3.12 illustrates the block diagram of the TSF method.

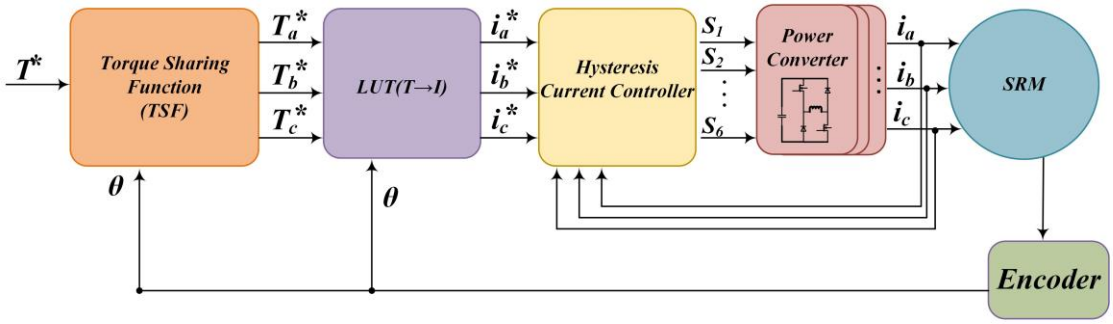

Figure 3. 12 The block diagram of the TSF torque control method.

The reference torque is divided into each phase using different distribution functions to produce ripple-free torque. The reference torque values in the TSF are defined as follows

$$T_{ref} = \begin{cases} 0 & 0 \le \theta < \theta_{on} \\ T_{ref}\, f_{rise}(\theta) & \theta_{on} \le \theta < \theta_{on} + \theta_{ov} \\ T_{ref} & \theta_{on} + \theta_{ov} \le \theta < \theta_{off} \\ T_{ref}\, f_{fall}(\theta) & \theta_{off} \le \theta < \theta_{off} + \theta_{ov} \\ T_{ref} & \theta_{off} + \theta_{ov} \le \theta < \theta_{p} \end{cases} \tag{3.15}$$

where, T_{ref}, f_{rise}, and f_{fall} represent the total reference torque, rising function for the incoming phase, and decreasing function for the outgoing phase, respectively. θ_{on}, θ_{ov}, θ_{off}, and θ_p are represented as turn on-angle, overlap angle, turn off-angle, and pole pitch, respectively. Pole pitch is defined as in (3.16), where the number of rotor poles is represented by Nr.

$$\theta_p = \frac{2\pi}{N_r} \tag{3.16}$$

The reference phase current is typically obtained using the *i(T, θ)* LUT, which is acquired through FEA. Among the conventional current control methods in SRMs, the hysteresis current control method is preferred due to its simplicity.

Existing literature categorizes conventional TSFs as linear and non-linear TSFs. Non-linear TSFs are further classified as cubic, sinusoidal, and exponential TSFs. Conventional TSFs are effectively used to minimize torque ripple in low-speed applications. However, at high-speed applications, torque ripple can increase due to current tracking errors, Figure 3.13.a and Figure 3.13.b show the linear and cubic TSF

curves, respectively. The commutation regions, where both adjacent phases are active, are Regions I and III. The reference torque is equally shared between the incoming and outgoing phases in these regions. However, Region II experiences single-phase conduction.

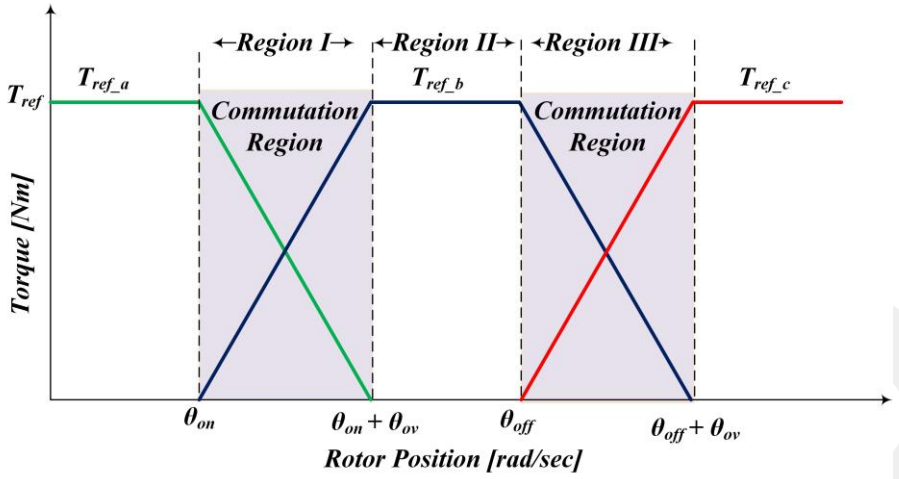

(a)

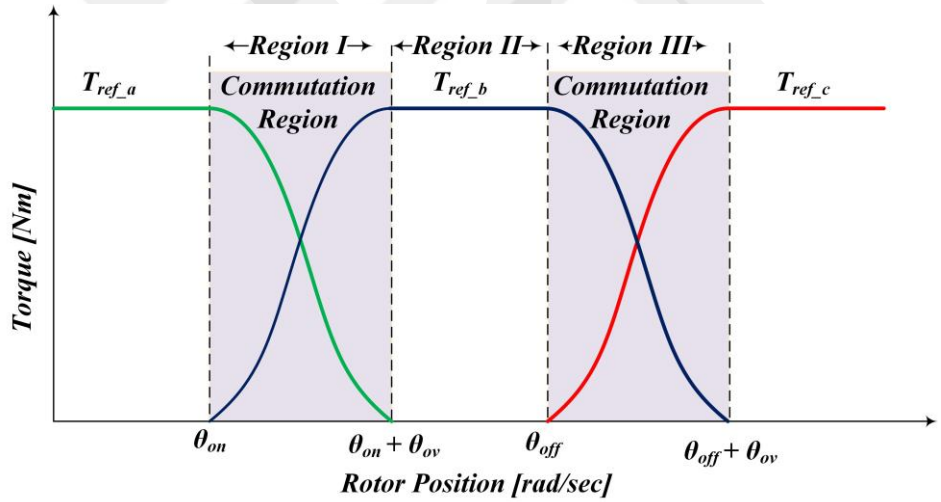

(b)

Figure 3. 13 (a) Linear TSF and (b) cubic TSF functions.

In linear TSF, the rising and falling functions of linear distributions can be formulated as

$$f_{rise}(\theta) = \frac{1}{\theta_{ov}}(\theta - \theta_{on})$$
$$f_{fall}(\theta) = 1 - f_{rise}(\theta + \theta_{on} - \theta_{off}) \quad (3.17)$$

where, the f_{rise} has to ascend from 0 to 1, while the f_{fall} has to descend from 1 to 0 during the commutation. Although the linear TSF can be used to control the torque, it may increase torque ripple due to the SRM's non-linear inductance profile, especially at the beginning and end of the commutation. To address this issue, the cubic TSF was introduced in the literature [46]. The rising and falling functions in the sinusoidal TSF are expressed as follows:

$$\begin{aligned} f_{rise}(\theta) &= \frac{1}{2} - \frac{1}{2}\cos\frac{\pi}{\theta_{ov}}(\theta - \theta_{ov}) \\ f_{fall}(\theta) &= 1 - f_{rise}\left(\theta + \theta_{on} - \theta_{off}\right) \end{aligned} \tag{3.18}$$

Here, a sinusoidal function is used to spread the torque throughout the consecutive phases.

In exponential TSF, one of the other TSF methods, the rising and falling functions are formulated as:

$$\begin{aligned} f_{rise}(\theta) &= (1 - \exp(\frac{-(\theta - \theta_{on})^2}{\theta_{ov}})) \\ f_{fall}(\theta) &= 1 - f_{rise}\left(\theta + \theta_{on} - \theta_{off}\right) \end{aligned} \tag{3.19}$$

Similar to other TSF methods, the torque in exponential TSF is distributed with an exponential function between consecutive phases, depending on the rotor position. The rising and falling functions in the cubic TSF are defined as follows:

$$\begin{aligned} f_{rise}(\theta) &= \frac{3}{\theta_{ov}^{\,2}}(\theta - \theta_{on})^2 - \frac{2}{\theta_{ov}^{\,3}}(\theta - \theta_{on})^3 \\ f_{fall}(\theta) &= 1 - f_{rise}\left(\theta + \theta_{on} - \theta_{off}\right) \end{aligned} \tag{3.20}$$

The cubic TSF method separates the torque produced by the consecutive phases using a cubic function in accordance with the rotor location, which is superior to other TSF methods [43]. However, this method may not be sufficient when the inductance characteristic of the SRM is highly nonlinear. In such cases, a more advanced TSF method, such as an adaptive TSF, may be required to achieve optimal torque control performance.

3.5 Conclusion

In this chapter, the working principle of SRM is mentioned and an explanation is given about how the machine works. SRM's driver topologies are briefly mentioned, and current and torque control methods are summarized.

Chapter 4

Torque Error Compensator Based TSF

4.1 Introduction

The minimization of torque ripple by the proposed TSF is presented here for the SRM considered. This proposed TSF is an online method where torque sharing is performed by cascading the TSF with a dynamic torque error compensator. The operation of the SRM beyond the base speed with remarkably mitigated torque ripple is possible by means of the proposed cascading torque-sharing strategy. The turn-off angle is defined based on the instantaneous speed and reference steady-state current. The proposed method is intended to take advantage of the fact that the outgoing phase produces the majority of the total torque and has a low time derivative of current due to the high inductance value. Therefore, the outgoing phase is maintained until it produces negative torque. The incoming phase is activated when it can produce a positive torque. The main purpose of the controller is to instantaneously estimate the output torque through LUTs and regulate the incoming stator phase current to compensate for the torque error. The details of the controller are explained in the next sections.

4.2 Control of The Outgoing Phase

The generated torque of the SRM is explained in Equation 3.11. The time derivative of inductance is linearly proportional to the torque produced and polarity. The phase current and inductance waveforms are shown in Figure 4.1; where, L_u, L_a, θ_{on}, θ_{off}, and θ_m are unaligned and aligned inductances, the turn-on/off angles, and the maximum angle for generating the positive torque, respectively. Torque control ability is restricted due to the high inductance level in the saturation region. However, compared to the incoming phase in the unsaturated region, the torque generation in the outgoing phase is higher than in the incoming phase. Hence, the outgoing phase should be arranged so as to produce

maximum torque. However, it is important to be cautious and make sure that the current in the phase does not go beyond the saturation region since the negative torque is produced when the phase current is available beyond the saturation region. Therefore, the outgoing phase angle where the phase current start diminishing should be carefully adjusted. Additionally, the power converter is operated in the demagnetization mode when the phase is turned off at a turn-off angle, θ_{off}; therefore, the compensating torque with the incoming phase becomes challenging. The reference current of the outgoing phase is slowly brought down to zero with a 2nd order low-pass filter (LPF) to fix the instantaneous torque dips that occur rapidly. The reason for preferring 2nd order LPF is that it reduces the reference current smoothly to zero. The parameters of the 2nd order LPF such as natural frequency and damping values have to be determined since these values are needed to describe how the current reference changes from its initial value to zero. Moreover, the natural frequency should be updated based on the instantaneous speed and reference steady-state current.

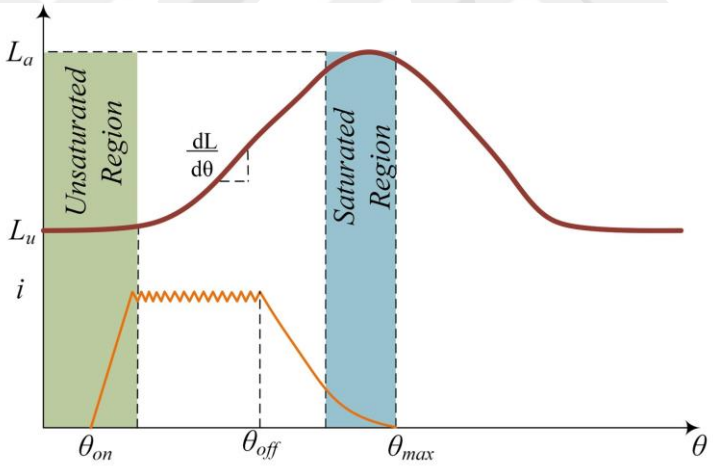

Figure 4. 1 The waveform of the inductance and current profile of an SRM.

The block diagram of the proposed cascade TSF method is shown in Figure 4.2. Here, the reference torque, T_{REF}, is converted to the reference steady state current via T-i-θ LUT. The reference current, abbreviated as I_{REF}^{SS}, is the maximum value that the current can reach when it is in single-phase conduction. The reference square wave raw currents represented as I_{a_raw}, I_{b_raw}, *and* I_{c_raw} are set based on the turn-on and turn-off angle in the commutation block. In the output of the LPF block, the raw reference currents symbolized as $I_{a\_raw}^{ref}$, $I_{b\_raw}^{ref}$, and $I_{c\_raw}^{ref}$ are obtained.

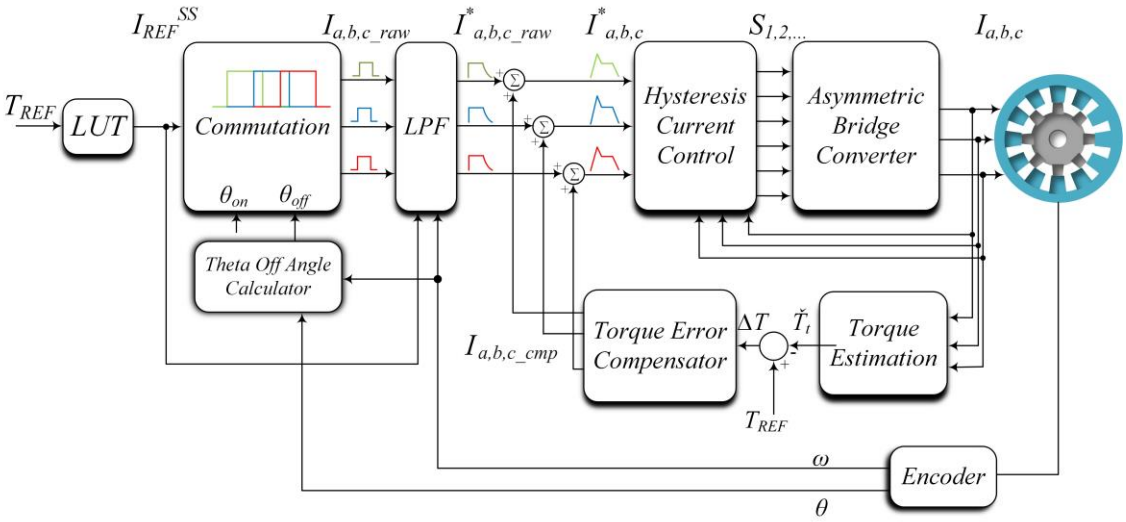

Figure 4. 2 Proposed control algorithm for SRM.

The one phase of the raw reference current is represented in Figure 4.3. In this figure, the theta-off region represents different turn-off angles at different speeds, θ_{off}^{I}, θ_{off}^{II}, and the settling times of the 2nd order LPF, T_s^I, T_s^{II}, means that how long it takes to bring the current down to zero. The settling time of the LPF is expressed as

$$T_s = \frac{-ln(tolerance\ fraction)}{2\pi\zeta f_n} \tag{4.1}$$

where, ζ and f_n represent the filter's damping ratio and natural frequency, respectively.

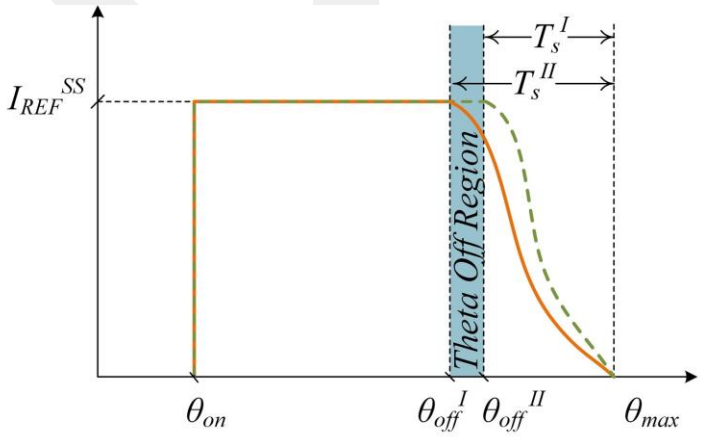

Figure 4. 3 Raw filtered reference current waveform in the proposed method.

The tolerance fraction is a coefficient representing the error band of the 2nd-order LPF and this value is selected as 0.02 for the most underdamped second-order filters. In the proposed method, the T_s is selected based on the instantaneous speed and reference

steady-state current; hence, the filter's natural frequency will change accordingly. The damping ratio and natural frequency parameters are utilized to react to the outgoing phase dynamics. These values should be optimized based on the speed and steady-state current obtained by using the parameter sweeping technique to enhance the torque ripple performance of the SRM. The damping ratio is chosen as 0.5 since this value supplies a smoother current reference at the beginning of the commutation; thus, prohibiting the torque ripple that can occur beginning of the commutation. After determining the optimal natural frequency varying according to the steady state current, I_{REF}^{SS}, and speed, ω, the optimal natural frequency is obtained using the second-order polynomial function as:

$$f_n = p_{00} + p_{10} \times I_{REF}^{SS} + p_{01} \times \omega + p_{11} \times I_{REF}^{SS} \times \omega + p_{20} \times \left(I_{REF}^{SS}\right)^2 + p_{02} \times \omega^2 \qquad (4.2)$$

where, p_{00}, p_{10}, p_{01}, p_{11}, p_{20}, and p_{02} are the polynomial coefficients which are 13.08, 0.5827, 0.8788, - 0.002949, -3.594×10-5, and -0.8147×10-7, respectively.

As soon as the settling time which is the distance where the current goes down to zero is calculated, the settling angle is then determined by multiplying the settling time and the speed. Then, the system calculates turn- off angle by subtracting the settling angle from the maximum operating angle, θ_{max}. The maximum operating angle in this case corresponds to the position where the phase inductance derivative with respect to the rotor position reaches a noticeably high negative value. In other words, it is the angle where negative torque generation increases when the current is still in the phase windings. As the settling time varies based on the instantaneous speed and reference steady-state current, different turn-off angles are obtained which are required for the adaptive control. The produce negative torque at the end of the commutation is eliminated, and better current tracking performance at the outgoing phase is achieved.

4.3 Torque Error Compensator

The current control dynamic in the unsaturated region is quicker than the saturation region since phase inductance is small. Therefore, instantaneous torque error for the SRM can be compensated by adjusting the incoming phase's current. In the proposed method, the raw reference current, $I^*_{a\text{-}b\text{-}c}$, is set as a steady-state value obtained by LUT to rise the actual current to generate the positive torque. However, it will not be used complementary to the outgoing phase to produce the torque. That’s why a second control system called a

torque error compensator is used to compensate for the torque error. The instantaneous torque can be either measured or estimated during the compensation. Since it is impossible to measure such torques coming from each phase, the only practical solution is to use an estimator. The estimator can be performed by means of either a mathematical model or LUTs. Taking into account, the SRM has a highly non-linear structure, the estimation process could be a long processing load in the mathematical model. Therefore, a torque estimation method base on LUT is applied to estimate the torque that produce by each individual phase. The produced torques by each individual phase are added and total torque estimation, $\check{T}_{total}$, is calculated. The torque error is determined by using the estimation torque and reference torque. This error value is converted to compensation phase current, $I_{a\text{-}cmp}$, $I_{b\text{-}cmp}$, $I_{c\text{-}cmp}$, based on the $i(T,\theta)$ LUT. Then, the obtained currents are summed with the raw reference current waveform and the reference current is getting so the error is minimized.

In summary, the phase currents are separated by the cascade torque-sharing control process. The turn-off angle is regulated according to the instantaneous speed and reference-steady state current to enhance the current tracking performance in the outgoing phase at first. Secondly, the incoming phase current is used to torque error compensation based on the instantaneous torque estimation and torque error. The better incoming current control performance is achieved during the torque error compensation process thanks to the small inductance value in the incoming phase; therefore, torque ripple is minimized successfully. Furthermore, the proposed method exhibits better performance in reducing torque ripple at high speeds in comparison to conventional methods.

4.4 Conclusion

To achieve minimized ripple operation for SRM, this chapter explains an online TSF that employs an instantaneous torque error compensation method. Unlike the existing TSF methods formulated with a mathematical expression, the proposed approach adjusts the shared torque between phases based on instantaneous torque error. The method takes advantage of the slow current dynamics of the outgoing phase due to high inductance and activates the incoming phase as soon as it can generate positive torque. During this process, total torque is estimated instantly using lookup tables, and a

correction current is calculated and added to the incoming phase reference current, considering the low inductance and fast current dynamics.

Chapter 5

Results and Discussion

5.1 Introduction

This chapter covers SRM modeling, simulation, and experimental study. The simulations are carried out on MATLAB/Simulink. The SRM is modeled using the LUTs obtained from the FEA, later, the traditional hysteresis current control, cubic TSF, and the proposed torque error compensation based TSF are simulated. Later, an experimental study is performed. The results were presented and compared to show the superiority of the proposed TSF method.

5.2 SRM Modeling

The SRM, parameters listed in Table 5.1, are used in this study.

Table 5. 1 Motor Specification.

Parameters	Value	Unit
Nominal power	1.25	kW
Nominal torque	12	Nm
Stator/rotor pole configuration	24/16	-
Number of phases	3	-
Base speed	1000	rpm
Rated voltage	200	Vdc

Required LUTs are obtained through FEA. The torque LUT, based on stator current and rotor location, is depicted in Figure 5.1, while the Flux Linkage LUT, which depends on stator current and rotor location, is presented in Figure 5.2. The Inductance LUT, which changes with stator current and rotor location, can be seen in Figure 5.3.

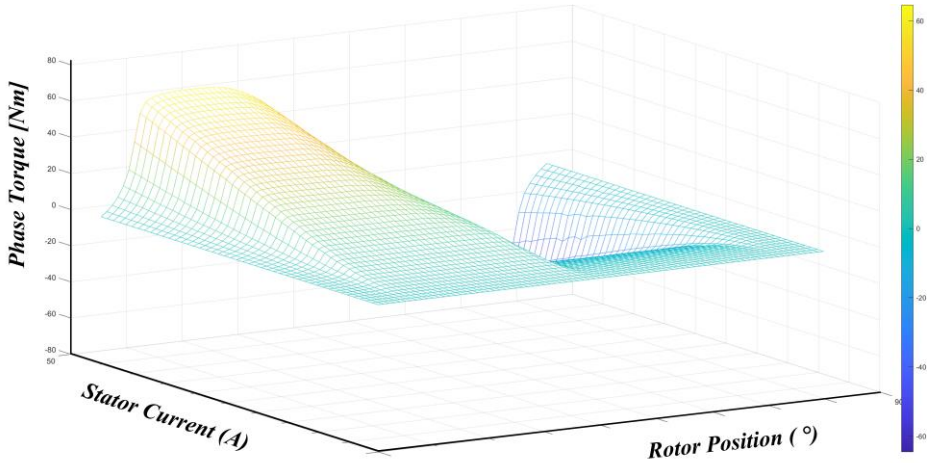

Figure 5. 1 Torque vs. current and position plot.

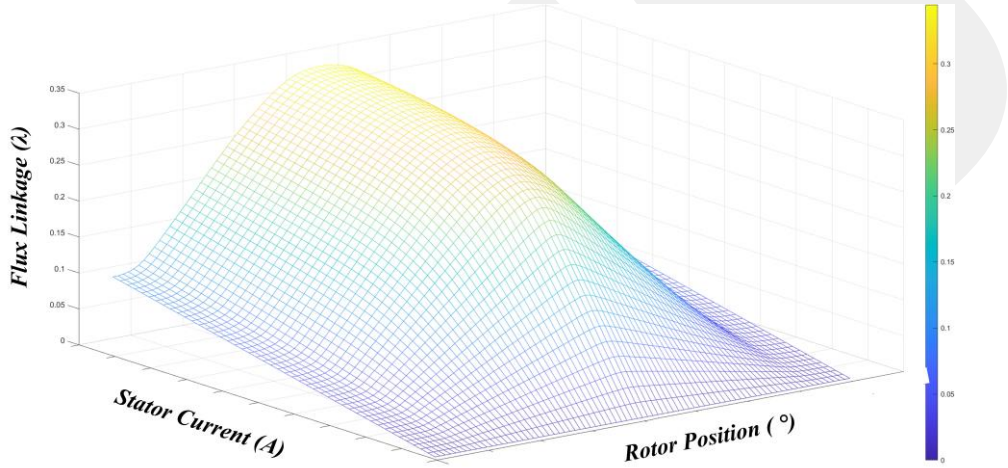

Figure 5. 2 Flux-linkage vs. current and position plot.

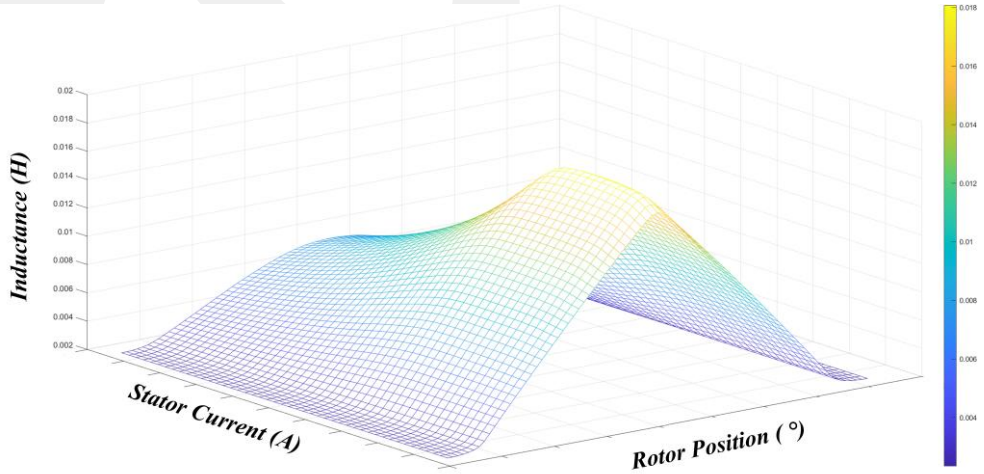

Figure 5. 3 Inductance vs. current and position plot.

The knowledge of both stator current and rotor location is necessary for the utilization of LUTs in SRM modeling. Figure 5.4 illustrates a block diagram of one-phase

SRM modeling. To obtain the position of the rotor, we need to first convert the reference speed from unit revolutions per minute (RPM) to radians per second by multiplying it by 60/2π. Next, we need to convert the rad/sec value to degrees/sec by multiplying it by π/30. This angular velocity is represented in degrees per second. The angular velocity is then integrated to obtain the rotor location, which is the first set of data needed for modulation.

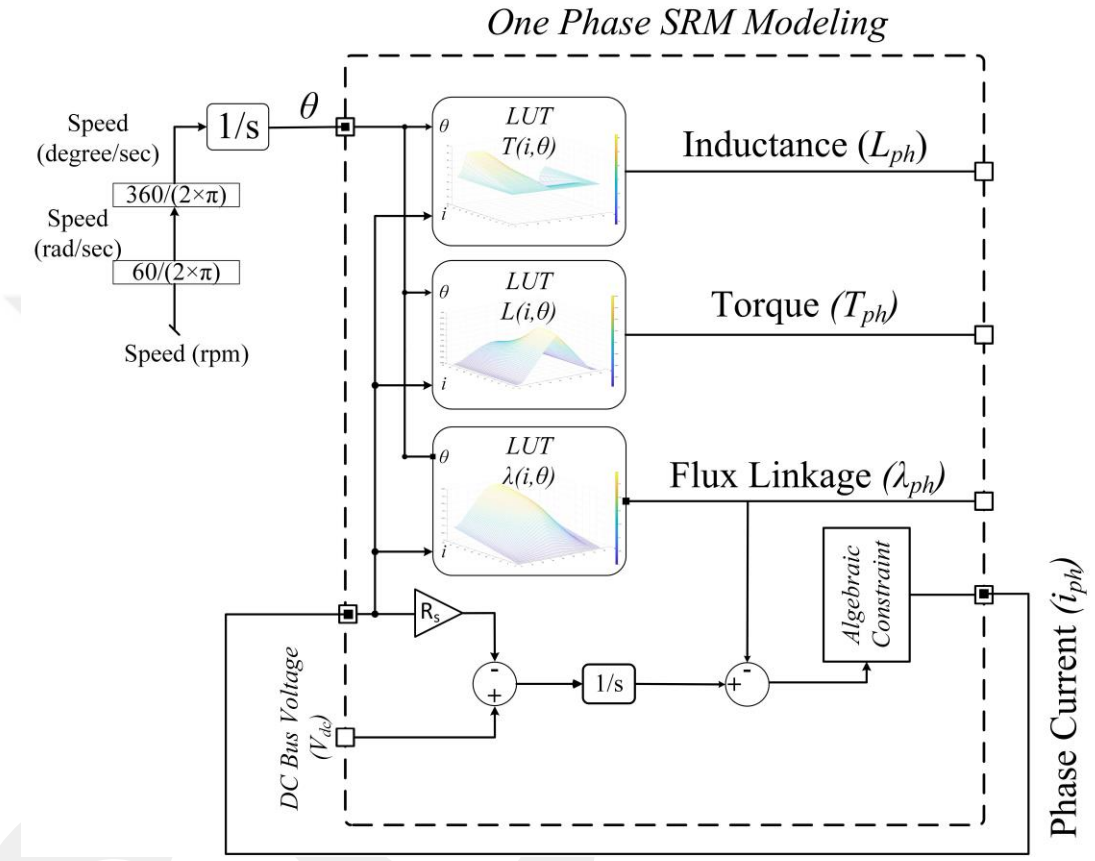

Figure 5. 4 SRM Modeling block diagram of the one phase.

The second set of data, i.e., the stator current, is obtained using the algebraic constraint block in the simulation platform, based on as follow:

$$\lambda_{ph} = \int (V_{dc} - i_{ph} \times R_s) dt \tag{5.1}$$

In order to solve Equation 5.1, phase current information is required, but the system's phase current is unknown. To address this issue, an algebraic constraint can be used to solve the system numerically using iterative methods like Newton-Raphson or Gauss-Seidel. The flux-linkage values obtained from the FEA method and the mathematical method are subtracted from each other, and the resulting system output is input the numerical solver's input. The numerical solver then produces an output value

that corresponds to the numerical solver's input zero. This output value is referred to as the phase current in the one-phase SRM model. This phase current is then multiplied by the stator resistance and used as a system input to determine the flux linkage.

5.3 Simulation Result

Initially, the SRM was controlled using hysteresis current control, which only regulates the region where a single phase is active and has no effect on torque ripple during commutation. For the commutation region, Cubic TSF was implemented.

5.3.1 Hysteresis Current Control

The block diagram of the hysteresis current control, as shown in Figure 5.5, separates the steady-state current, I_{REF}^{SS}, into three-phase raw currents based on the turn-on and turn-off angle in the commutation period. For this simulation, the turn-on angle (θ_{on}) and turn-off angle (θ_{off}) were selected as 7.5° and 15°, respectively, and an asymmetric bridge converter applying hard chopping was chosen as the power converter. The sampling time and hysteresis band were set to 12 μs and 0.2, respectively, to minimize torque ripple. The simulation was conducted at the base speed of 1000 rpm, and a torque ripple of 68% was observed for the hysteresis control at the base speed. Torque waveforms were recorded, and the torque ripple, T_{ripple}, was calculated.

$$T_{ripple} = \frac{T_{\max} - T_{\min}}{T_{avg}} \tag{5.2}$$

where T_{max}, T_{min}, and T_{avg} are the maximum, minimum, and average torque of the SRM, respectively.

The waveforms of stator phase currents, phase torques, and total torque are presented in Figure 5.6. It is apparent that there is no control in the commutation region, resulting in a very high current tracking error. This high tracking error leads to increased torque ripple. Therefore, the control of the SRM is primarily focused on the commutation period to minimize the current tracking error and reduce torque ripple.

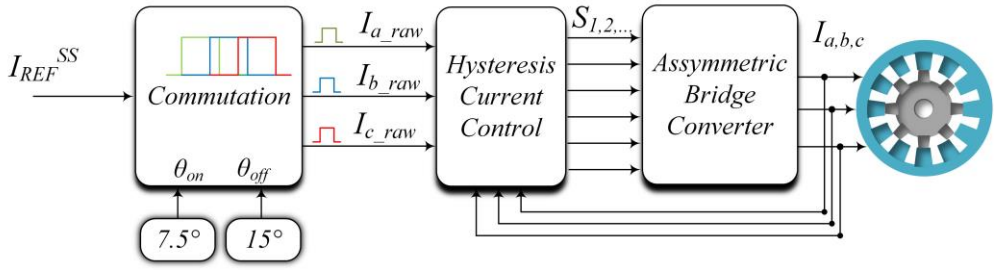

Figure 5. 5 Schematic of the Hysteresis Current Control Algorithm.

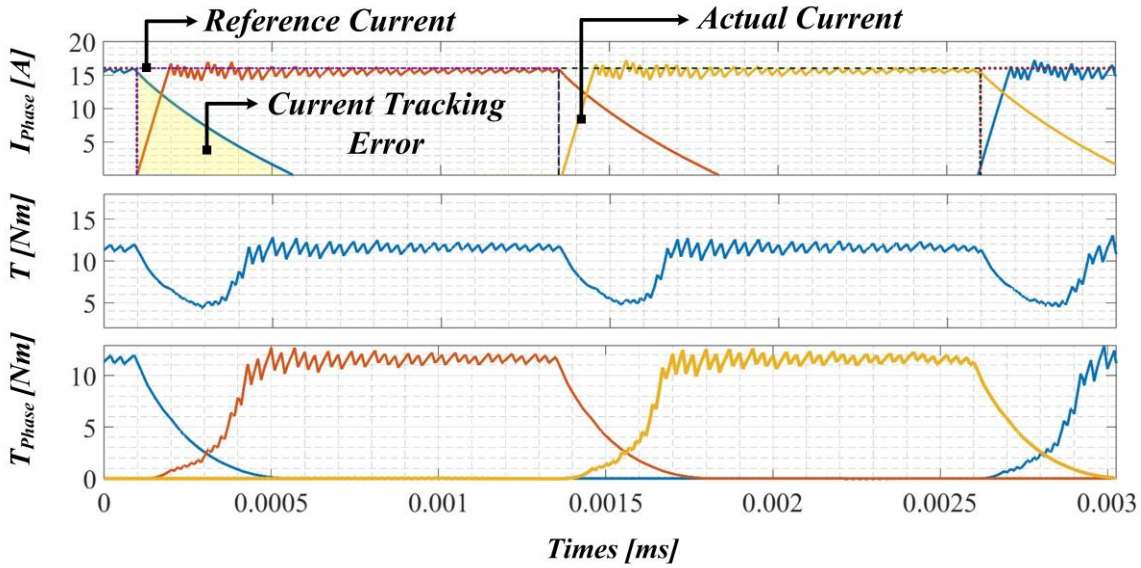

Figure 5. 6 Hysteresis current control behavior for SRM.

5.3.2 Cubic Torque Sharing Function

The TSF approach is mainly aimed at controlling the commutation region by separating torque based on a mathematical expression. Details of the TSF can be found in section 3.4.2.4. The block diagram of the TSF is shown in Figure 3.12. During the verification process, the Cubic TSF method was chosen as it outperformed other conventional TSF methods [43]. The reference torque is separated into three phases using the mathematical expression described in Equation 3.20, and the inverse LUT *i(T-θ)* is used to convert the reference phase torque to reference phase current. The sampling time and hysteresis band were selected in a similar manner to the hysteresis current control.

The waveforms of the conventional cubic TSF for motor operation at 400, 1000, and 1200 rpm are presented in Figure 5.7, Figure 5.8, and Figure 5.9, respectively. These waveforms show the stator phase current, phase torque, and total torque of the motor. The turn-on, overlap, and turn-off angles are manually adjusted for each speed level to reduce torque ripple and RMS input current during the commutation period, with values set at 7.5°, 2.5°, and 15°.

The turn-on, overlap, and turn-off angles are manually adjusted as 7.5°, 2.5°, and 15°, respectively, across all speed levels to minimize torque ripple and RMS input current during the commutation period. The waveform of the cubic TSF when the motor operates at 400 rpm is presented in Figure 5.7. At low speeds, the phase stator current can track the reference current due to the low absolute Flux derivation values, resulting in a torque ripple of only 5%.

Figure 5.8 presents the waveform of the cubic TSF at the base speed of 1000 rpm. As the speed increases, the absolute value of the flux derivation increases. As a result, the cubic TSF's ability to track current deteriorates. Consequently, the error and torque ripple increase, as illustrated in Figure 5.8. The torque ripple when the motor runs at the base speed is calculated as 27%, while the maximum stator phase current is observed to be 28A.

The effectiveness of the Cubic TSF is also evaluated above the base speeds, specifically at 1200 rpm. The torque ripple was recorded as 32%, and the high current tracking error resulted in high peak phase currents, as shown in Figure 5.9.

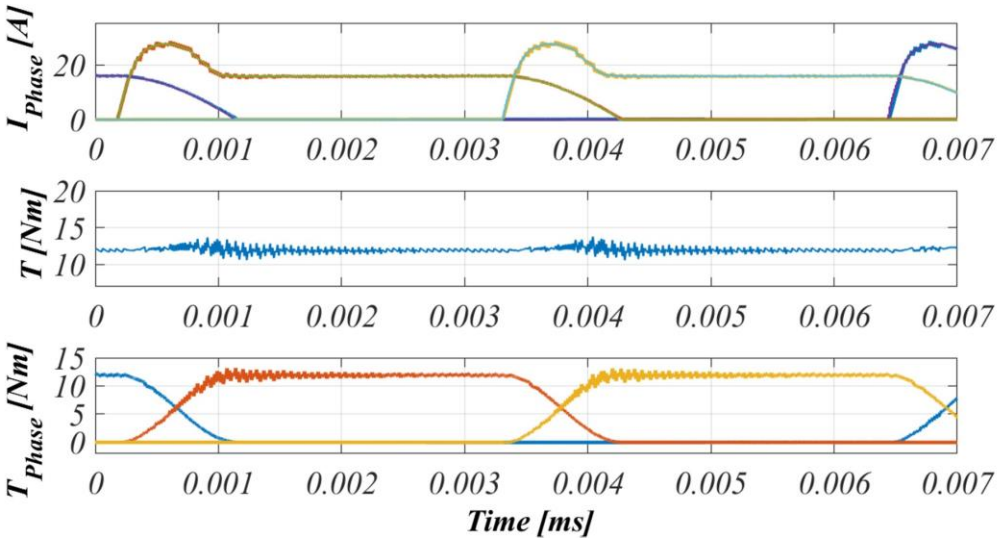

Figure 5. 7 Simulation result Cubic TSF at 400 rpm.

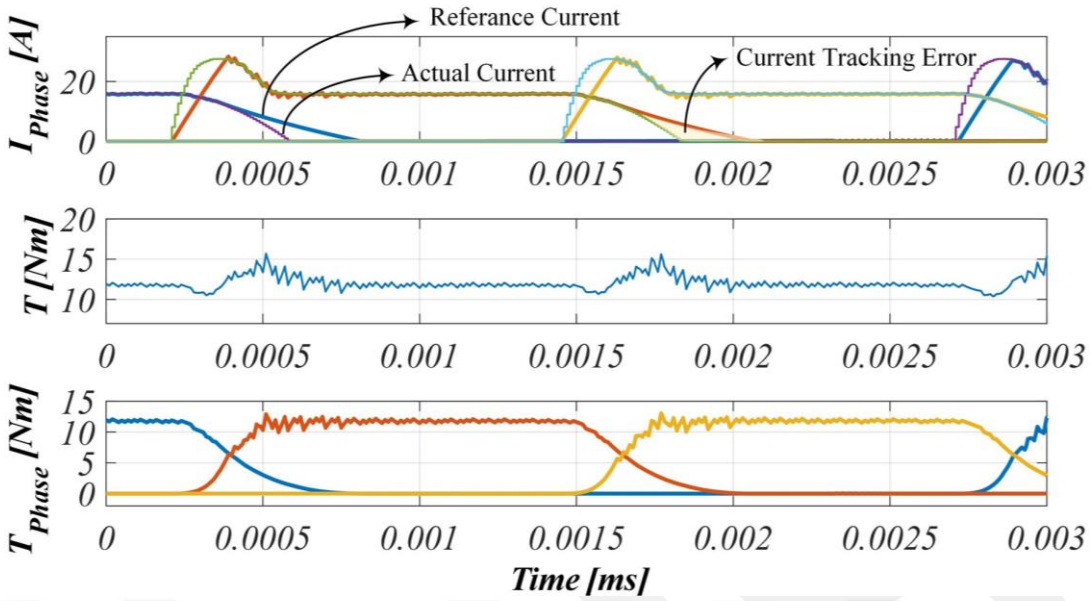

Figure 5. 8 Simulation result Cubic TSF at 1000 rpm.

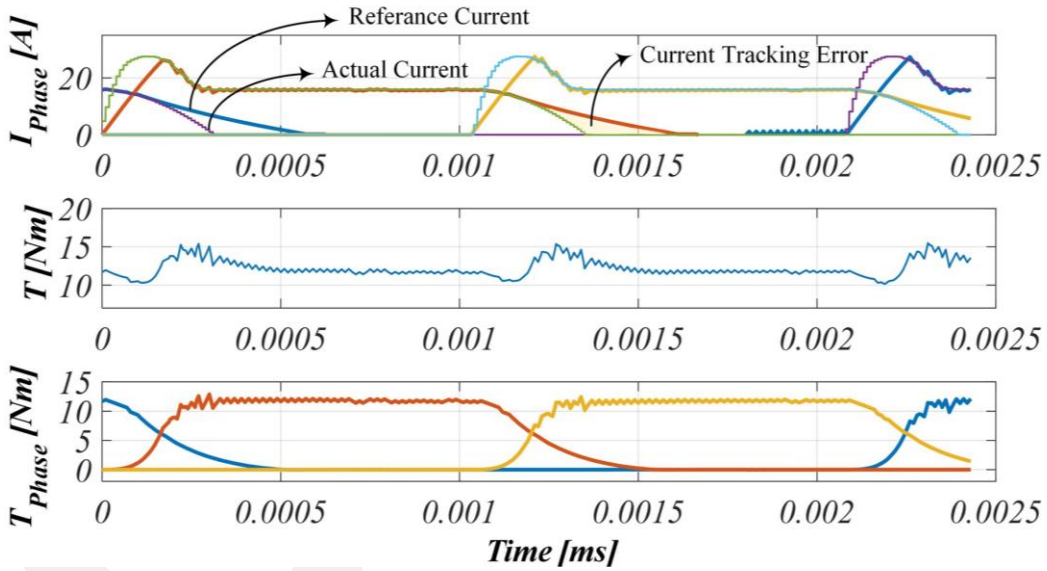

Figure 5. 9 Simulation result Cubic TSF at 1200 rpm.

5.3.3 Proposed TSF Method

The simulation was performed in MATLAB®/Simulink. The hysteresis band limit is arranged as ± 0.2 A and the sampling time is used 12 μs such as other simulation performances.

In Figure 5.10, Figure 5.11, and Figure 5.12 the waveforms of the proposed method when the motor runs at 400, 1000, and 1200 rpm are indicated, respectively. These waveforms show phase currents, phase torques, and total torque, respectively.

The turn-on angle in the proposed method is arranged to 7.1° where this angle is represented the minimum inductance value that can generate positive torque. In the proposed method, the turn-off angle that varies based on instantaneous rotor speed and steady-state reference current are determined as 15.61°, 15.13°, and 15.05° for 400, 1000, and 1200 rpm speeds, respectively.

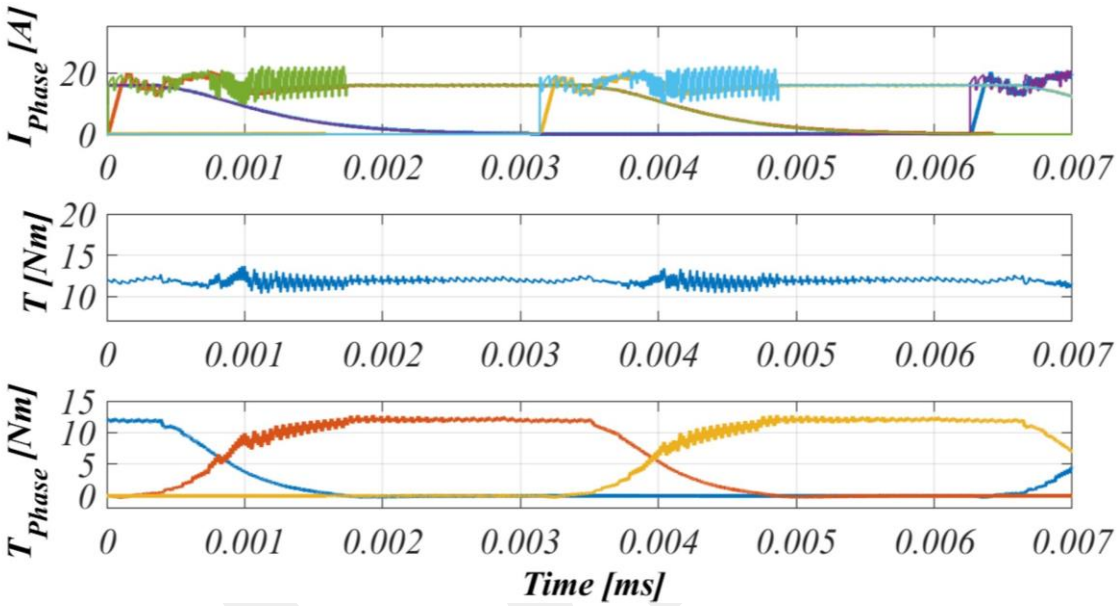

Figure 5. 10 Simulation results proposed method at 400 rpm.

Figure 5.10 is shown the waveform of the proposed method when the motor operates at 400 rpm. The phase currents can be easily tracking the reference current at this speed; hence, torque ripple is calculated as 5% similar to the cubic TSF presented in Figure 5.7. However, compared to the maximum phase current, cubic TSF is surpassed 20 A whereas, the proposed method is reaching to 20A. Therefore, although both control approach at 400 rpm has a similar torque ripple, the copper loss is lower than in the proposed method.

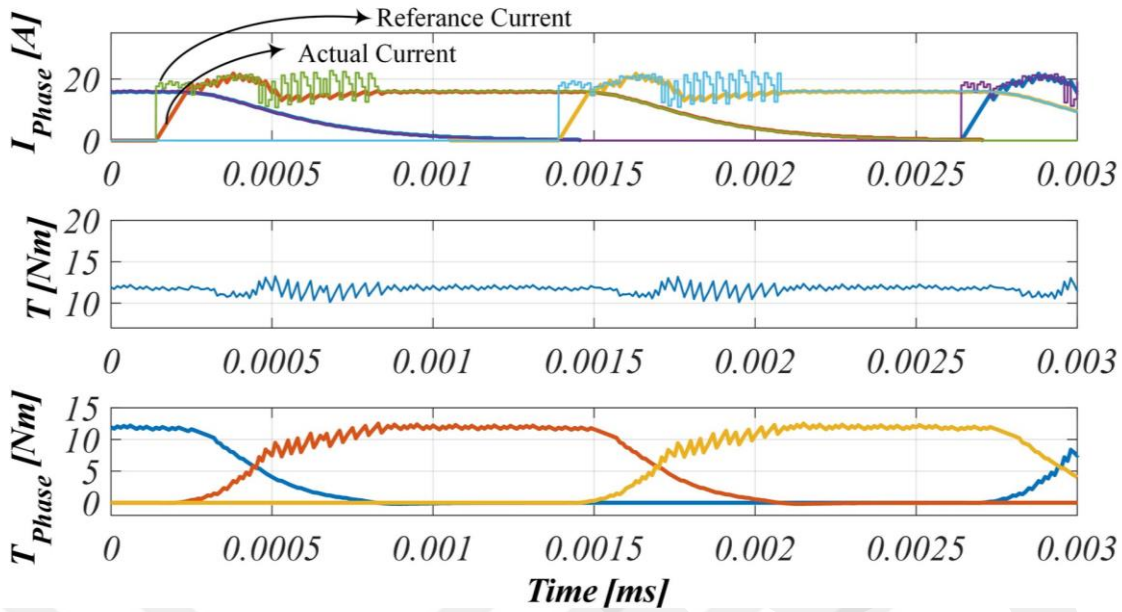

Figure 5. 11 Simulation results proposed method at 1000 rpm.

The waveform of the proposed method at the base speed,1000 rpm, is shown in Figure 5.11. Despite, the absolute flux derivation value increasing as the speed increases, the reference current tracking capability is resulting better than cubic TSF was performed at the base speed provided in Figure 5.8. Thanks to the changed turn-off angle and compensating for the torque error, the proposed method results in better current tracking capability; hence, torque ripple and the peak current are brought down from %27 to 9%, and from 28 A to 22 A, respectively.

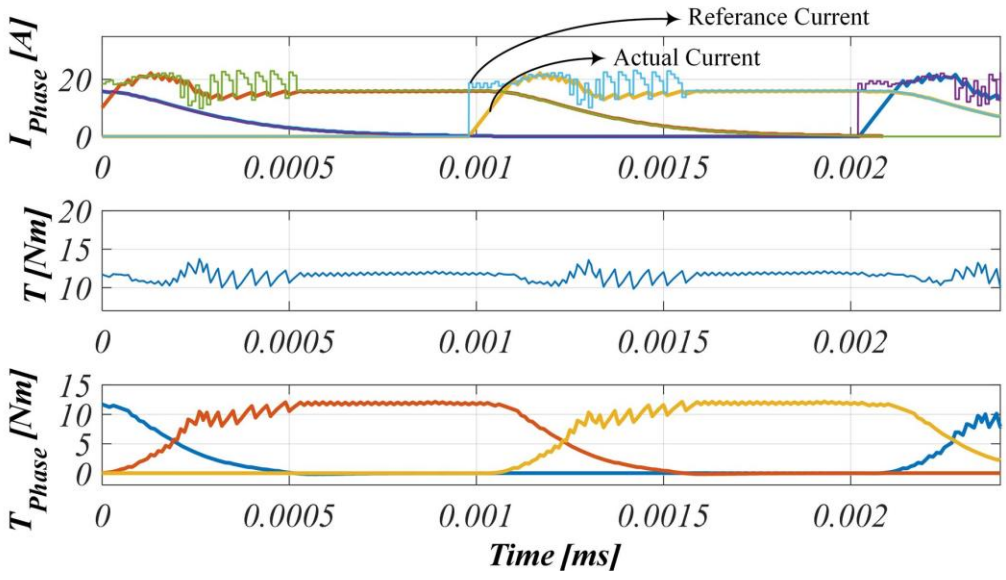

Figure 5. 12 Simulation results proposed method at 1200 rpm.

The proposed method is conducted above the base speed, 1200 rpm as shown in Figure 5.12. The torque ripple is still reserved under the 11% with the proposed method, and also current reach 23 A phase current. Compared to the cubic TSF indicated in Figure 5.9, the torque ripple and maximum phase current significantly reduce at the high-speed application.

According to the simulation findings, thanks to the better current tracking performance with a small tracking error and torque error compensating with the incoming phase, the proposed method successfully minimized torque ripple and peak currents. As speed increases, increase the current tracking error is eliminated with an adaptive turn-off angle. Thus, the maximum efficiency is obtained from the outgoing phase.

Consequently, the proposed method performed better than the cubic TSF in the different speed applications.

5.4 Test Rig

The experimental work is realized to validate the proposed method. The test system consists of a dynamometer system. This dynamometer system includes a loading machine that has a motor-driven unit that operation of the speed control mode, a torque transducer, an oscilloscope, current probes, a device under test (SRM), and its driven unit. The block diagram and photograph of the test system are provided in Figure 5.13 and Figure 5.14, respectively.

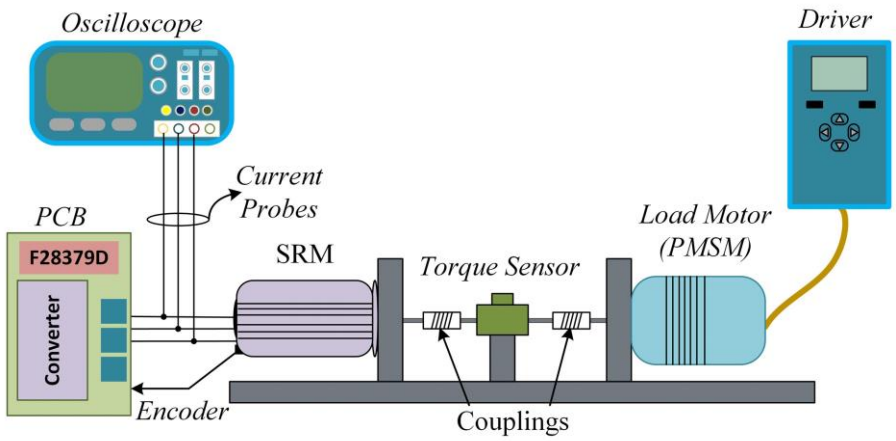

Figure 5. 13 Block diagram of the test system.

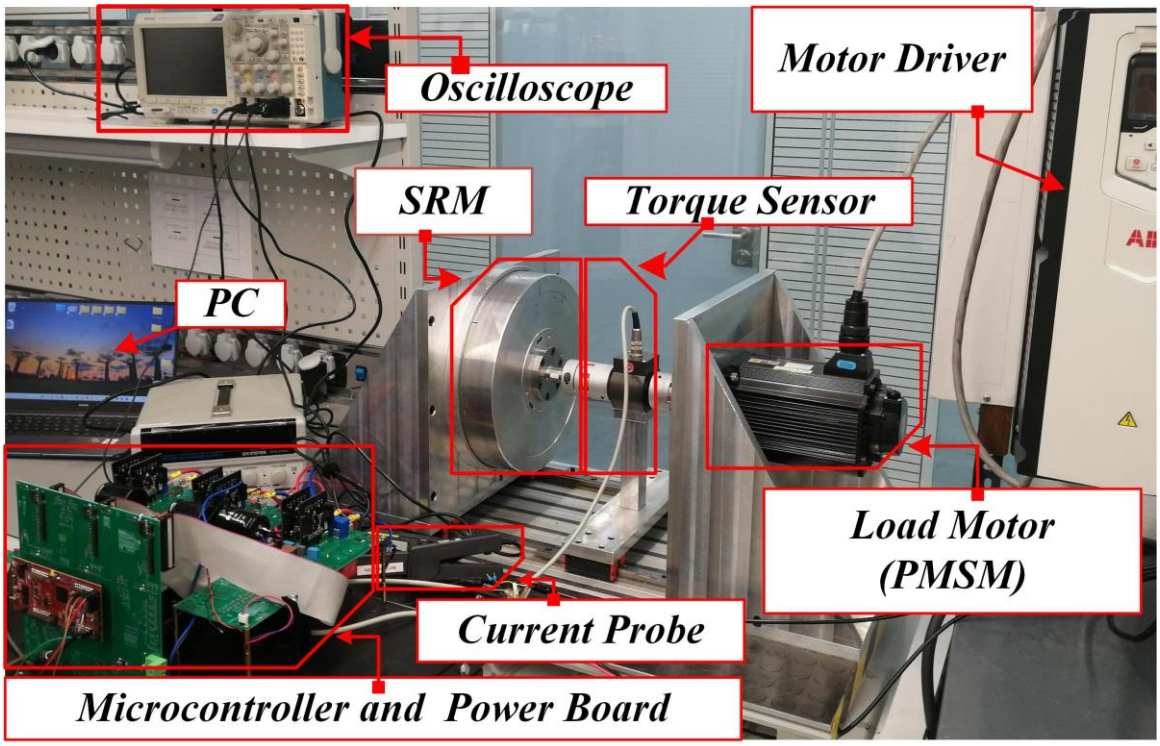

Figure 5. 14 The experimental setup of the proposed method.

The asymmetric bridge converter having SiC MOSFETs called SRM driven unit is used to control the current with the hysteresis current control method, and the band of the hysteresis current controller is set as 0.2 A similar to the simulation studies. A Texas Instruments TMS320F28379D MCU with has 12 µs control period is used during the verification process. The instantaneous speed and rotor location feedback of the SRM are determined by the A 1000-pulse quadrature encoder. The phase currents are captured with current probes named Tektronix A622 and the torque transducer signal is measured with the voltage probes. Tektronix MDO3014 100 MHz oscilloscope is used for the observation of these signals.

5.5 Experimental Results and Discussion

Experiment works are performed at the low, base, and high speeds applications. The torque ripple and phase currents waveforms are inspected during the verification process of the proposed method.

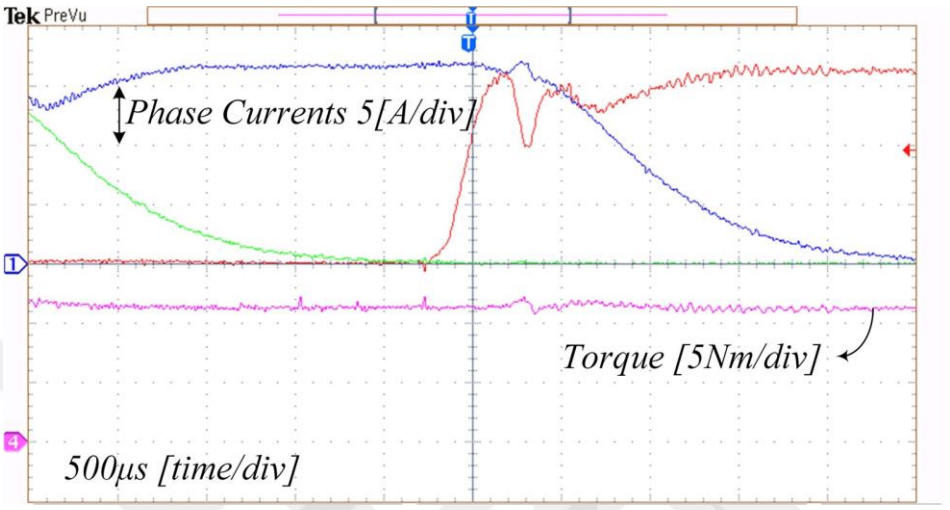

Figure 5. 15 Experiment result of the proposed method at 400 rpm.

Figure 5.15, the phase currents and output torque are presented when the machine is operated at 400 rpm. It is indicated fromthe waveform that the torque ripple calculates as 8% and the peak current observes as 16 A. Then, the motor is operated at the base speed, 1000 rpm, and the waveform is given in Figure 5.16. The peak phase current is noted as 18.5 A, whereas the torque ripple and average torque are noted as 15% and 12 Nm, respectively.

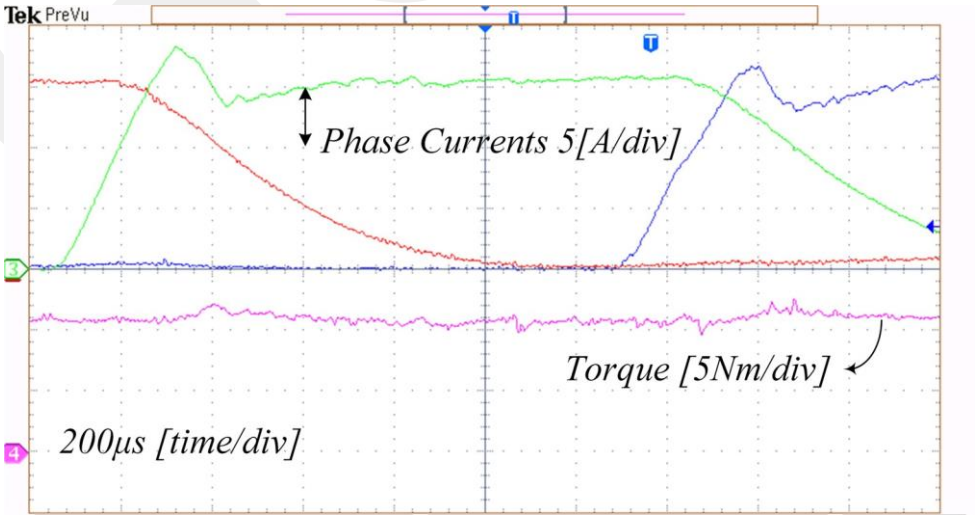

Figure 5. 16 Experiment result of the proposed method at 1000 rpm.

The proposed method is also performed at high speeds to assess performance. Figure 5.17 and Figure 5.18 indicated the waveform of the phase currents and torque, respectively. The average and output torque are remarked as 11.5 Nm, 21%, and 18A during the runs at 1200 rpm; additionally, these values are observed as 9.5 Nm, 29%, and 17.5 A, respectively.

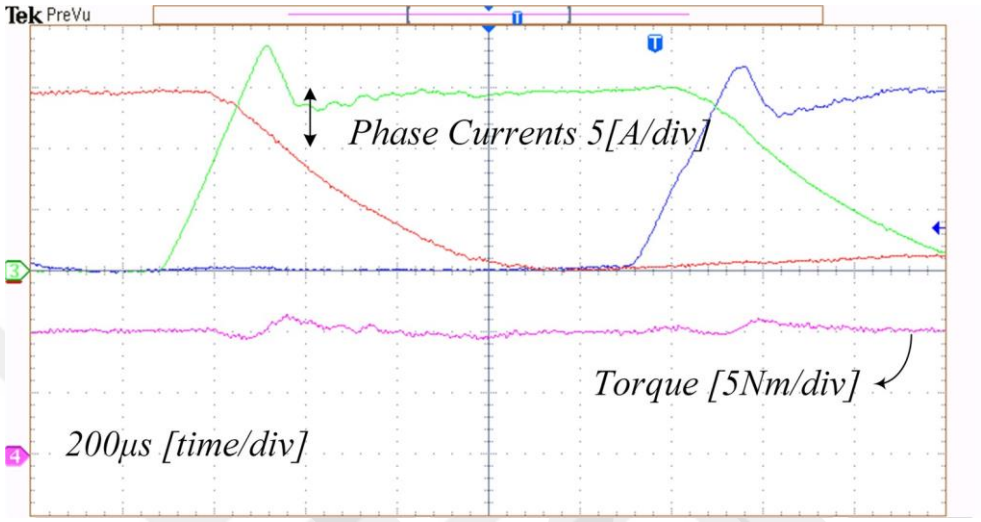

Figure 5. 17 Experiment result of the proposed method at 1200 rpm.

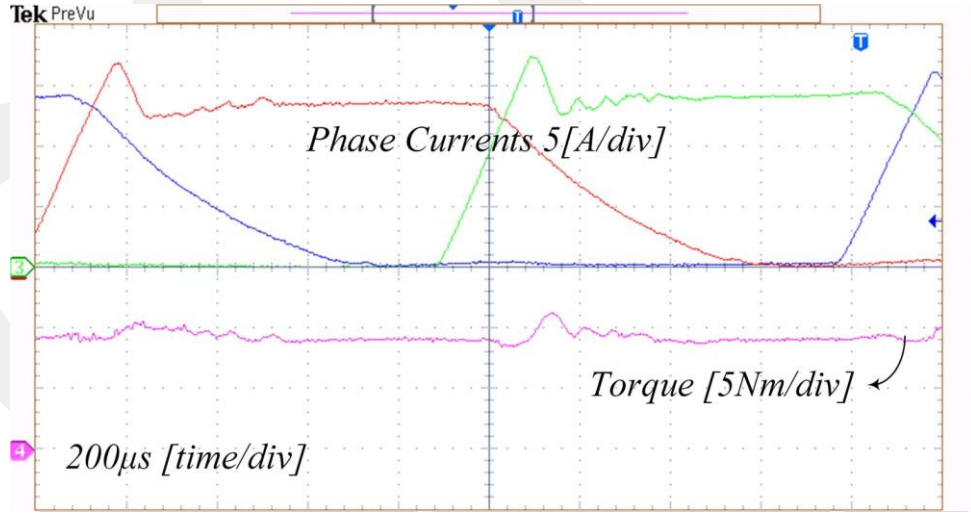

Figure 5. 18 Experiment result of the proposed method at 1400 rpm.

Since low flux linkage derivation values, almost identical torque control performance is observed in cubic and proposed TSF during the low-speed application verification. However, as the speed increase, the proposed method accomplishes lower torque ripple. The main problem with conventional TSF is that the torque sharing between

consecutive phases becomes challenging as speed increases; hence, tracking the reference phase current becomes impossible with the mathematical expression at a certain speed limit. To fix this problem, the proposed TSF controls the torque based on the adjusted turn-off angle and compensates for the torque error. The torque ripple is compared in Figure 5.19. The blue line, green line, and red line are represented cubic TSF simulation, proposed method simulation, and proposed method experiment, respectively. As speed increases, the proposed method achieves lower torque ripple than cubic TSF as seen in Figure 5.19.

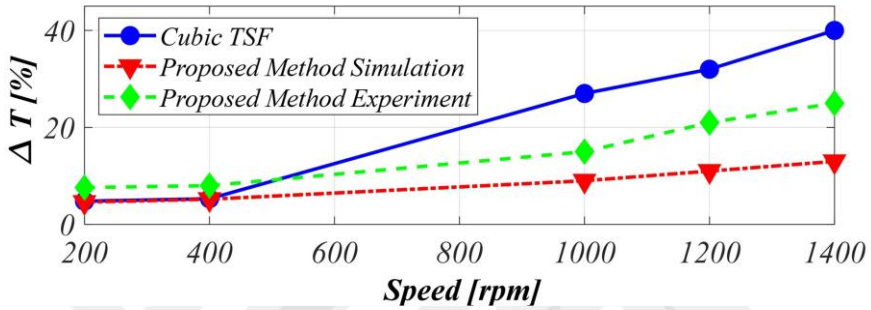

Figure 5. 19 The comparison of torque ripple in each presented method.

5.6 Conclusion

In this chapter, the proposed TSF method and the conventional cubic TSF, and conventional hysteresis current control methods are compared by means of torque ripple performances. First, all methods were simulated using LUT based SRM model. Later, the proposed method is validated with an experimental study. Classical hysteresis control demonstrated poor torque ripple performance even at low-speed regions. Cubic TSF and proposed TSF methods demonstrate similar torque ripple performance at speeds below the base speed, with a calculated value of approximately 5%. However, as the speed increases, the proposed method takes the superiority over to the cubic TSF thanks to its torque error compensator and turn-off angle adaptation mechanism. The cubic TSF exhibits a torque ripple of 27%, while the proposed method achieves a significantly lower value, 9%, at the base speed. Above the base speed, minimizing torque ripple becomes more challenging, and current tracking performance plays a crucial role. To validate the effectiveness of the proposed method, experimental studies are conducted over the operating speed range, torque ripple values are recorded as 8%, 15%, 21%, and 29% at 400 rpm, 1000 rpm, 1200 rpm, and 1400 rpm, respectively. It should be noted that the

experimental torque ripple results are slightly higher than the simulation results due to various factors such as the measurement noise and discrepancies between the FEA model and the built motor.

Chapter 6

Conclusion and Future Prospects

6.1 Conclusion

This thesis comprises six distinct chapters, each of which contributes to the discussion surrounding the development and use of Switched Reluctance Machines (SRMs) in the field of electrical machines. In Chapter I, the research question and thesis statement are introduced, with a particular focus on the challenges of torque ripple in SRMs. Despite their increasing importance in the quest for more environmentally friendly and efficient machines, SRMs remain less favored than other machine types due to their poor torque ripple performance. The chapter ends by highlighting the torque sharing function technique (TSF) as a potential solution to this challenge.

Chapter II discusses the use of switched reluctance motors (SRMs) in industry and their advantages and disadvantages. One major advantage is their low manufacturing cost, while a disadvantage is their high torque ripple. To mitigate this ripple, researchers have looked into the optimization of firing angles and torque control techniques. This chapter also presents a literature survey about the torque control approach aimed to mitigate torque ripple. The torque sharing function is thoroughly examined, and its advantages and disadvantages are discussed. The chapter concludes by highlighting its common use and preference in the industry.

Chapter III provides an in-depth discussion of the working principle of SRMs, along with an overview of their driver topologies and current and torque control methods. The chapter also covers the key benefits and drawbacks of SRMs, as well as their various applications in different industries. The chapter ends with delve explanation of the torque control methods.

Chapter IV presents the proposed torque-sharing method based on instantaneous torque error compensation for SRMs. The conventional torque sharing function (TSF) shares the torque with consecutive phases based on a mathematical expression. In contrast, in this thesis, an instantaneous torque-sharing method is proposed based on the instantaneous speed and reference steady-state current without relying on any mathematical expression. The main objective of the controller is to achieve efficient torque generation from the outgoing phase whenever possible, considering that the inductance profile is high and the current dynamic rate is slow. To achieve this, a second-order low-pass filter (LPF) is implemented to designate the curve of the outgoing phase. The LPF's cutoff frequency and turn-off angle are optimized to avoid negative torque production. The turn-on angle of the incoming phase is set at the earliest angle where positive torque can be generated. The compensation current is calculated using look-up tables (LUTs) based on the instantaneously estimated torque and added to the filtered reference current to obtain the reference current during this process. Consequently, the SRM exhibits reduced torque ripple performance at an extended speed range.

Therefore, the adaptive torque-sharing technique proposed in this thesis has been shown to reduce torque ripple at an extended-speed region. The performance of this approach has been demonstrated through both simulation and practical studies. At low-speed applications, the proposed method exhibits similar performance to the cubic TSF. However, at high-speed applications, the proposed method shows superior torque ripple performance.

The proposed TSF method, the conventional cubic TSF, as well as the conventional hysteresis current control performances are compared in terms of torque ripple in Chapter V. According to the simulations, the proposed method and cubic TSF have similar torque ripple performance at speeds below the base speed, while the proposed method outperforms cubic TSF at higher speeds. Experimental results validate the effectiveness of the proposed method in reducing torque ripple.

6.2 Societal Impact and Contribution to Global Sustainability

Electric motors are essential for modern life, powering everything from household appliances to industrial machinery. However, they also consume a significant amount of energy and contribute to greenhouse gas emissions. In order to address these issues, this thesis emphasizes the importance of improving the performance of electric motors by means of mitigating torque ripple, particularly in SRM to promote sustainable development. Torque ripple is a phenomenon that occurs when the torque output of an electric motor oscillates, leading to decreased efficiency, increased noise, and vibration, and reduced overall performance. By developing control algorithms and other technologies to mitigate torque ripple, the researchers can improve the efficiency and performance of electric motors. This, in turn, reduces energy consumption and carbon emissions, making electric motors more sustainable and environmentally friendly.

SRM has emerged as a promising alternative to traditional permanent magnet motors, as they can eliminate the rare earth materials required for motor production. Rare earth materials are critical components in many types of electric motors, but their extraction and processing can have significant environmental impacts. By reducing the need for these materials in motor production, researchers can promote sustainable resource use and minimize the environmental impact of electric motor production.

Additionally, this thesis highlights the need for continued research and development in these areas to further advance sustainable motor technologies. In summary, this thesis underscores the importance of improving electric motor performance to promote sustainable development. By developing control algorithms and other technologies, as well as utilizing SRMs, researchers can make significant contributions to global sustainability while also improving the efficiency and performance of electric motors. The reduction of rare earth materials and energy consumption is crucial to achieving sustainable development and minimizing the environmental impact of electric motor production.

6.3 Future Prospects

This thesis presented a new torque-sharing method based on instantaneous torque error compensation SRM. The research can also direct to the following future prospects:

- Investigate the feasibility of using machine learning techniques for the TSF adaptation mechanism to improve performance and reduce complexity.
- Investigating the effectiveness of applying advanced optimization techniques for enhancing the efficiency and performance of the TSF control system.
- Investigate the use of advanced motor drive topologies that can be used with the proposed TSF to further improve the SRM performance in a wider speed range.

BIBLIOGRAPHY

[1] Z. Xia, G. Fang, D. Xiao, A. Emadi, and B. Bilgin, "An Online Torque Sharing Function Method Involving Current Dynamics for Switched Reluctance Motor Drives," *IEEE Transactions on Transportation Electrification*, pp. 1–16, 2022, doi: 10.1109/TTE.2022.3183171.

[2] IEA 2022, "Breakthrough Agenda Report 2022," Paris, 2022. Accessed: Feb. 25, 2023. [Online]. Available: https://www.iea.org/reports/breakthrough-agenda-report-2022

[3] 4E Electric Motor Systems Annex, "Policy Guidelines for Motor Driven Units," 2018. [Online]. Available: www.motorsystems.org

[4] L. Ge, B. Burkhart, and R. W. de Doncker, "Fast Iron Loss and Thermal Prediction Method for Power Density and Efficiency Improvement in Switched Reluctance Machines," *IEEE Transactions on Industrial Electronics*, vol. 67, no. 6, pp. 4463–4473, Jun. 2020, doi: 10.1109/TIE.2019.2922937.

[5] A. Klein-Hessling, B. Burkhart, and R. W. de Doncker, "Iron Loss Redistribution in Switched Reluctance Machines Using Bidirectional Phase Currents." [Online]. Available: http://www.isea.rwth-aachen

[6] Q. Ma, D. Bi, and B. Ge, "Digital control issue of high speed switched reluctance motor," *IEEE International Symposium on Industrial Electronics*, pp. 641–646, 2012, doi: 10.1109/ISIE.2012.6237164.

[7] B. Bilgin, J.W. Jiang, and A. Emadi, *Switched Reluctance Motor Drivers*. Boca Raton: CRC Press/Taylor & Francis Group, 2019. [Online]. Available: https://doi.org/10.1201/9780203729991.

[8] I. Husain, "Minimization of torque ripple in SRM drives," *IEEE Transactions on Industrial Electronics*, vol. 49, no. 1, pp. 28–39, 2002, doi: 10.1109/41.982245.

[9] A. Dorneles Callegaro, J. Liang, J. W. Jiang, B. Bilgin, and A. Emadi, "Radial force density analysis of switched reluctance machines: The source of acoustic noise," *IEEE Transactions on Transportation Electrification*, vol. 5, no. 1, pp. 93–106, 2019, doi: 10.1109/TTE.2018.2887338.

[10] J. W. Lee, H. S. Kim, B. il Kwon, and B. T. Kim, "New rotor shape design for minimum torque ripple of SRM using FEM," *IEEE Trans Magn*, vol. 40, no. 2 II, pp. 754–757, 2004, doi: 10.1109/TMAG.2004.824803.

[11] P. Bober and Ž. Ferková, "Online Optimization of Firing Angles for Switched Reluctance Motor Control," *International Conference on Electical Drives and Power Electronics*, pp. 238–242, 2021, doi: 10.1109/EDPE53134.2021.9604057.

[12] L. al Quraan, "Adaptive Firing Angles Control for Switched Reluctance Motor," pp. 119–124, 2023.

[13] Y. Wang, H. Wu, W. Zhang, and Y. Ma, "A high efficiency direct instantaneous torque control of SRM using commutation angles control," in *2014 17th International Conference on Electrical Machines and Systems, ICEMS 2014*, 2014, pp. 2863–2866. doi: 10.1109/ICEMS.2014.7013985.

[14] R. B. Inderka and R. W. A. A. de Doncker, "DITC - Direct Instantaneous Torque Control of Switched Reluctance Drives," *IEEE Trans Ind Appl*, vol. 39, no. 4, pp. 1046–1051, Jul. 2003, doi: 10.1109/TIA.2003.814578.

[15] C. Y. Yang, C. Bao, S. J. Song, Q. Y. Cheng, J. X. Zhong, and C. Y. Liu, "High Dynamic Direct Instantaneous Torque Control of Switched Reluctance Machine Based on Magnetic Co-energy Torque Estimation," in *2022 International*

Conference on Electrical Machines and Systems, ICEMS 2022, 2022. doi: 10.1109/ICEMS56177.2022.9983373.

[16] M. V. de Paula and T. A. D. S. Barros, "A sliding mode ditc cruise control for srm with steepest descent minimum torque ripple point tracking," *IEEE Transactions on Industrial Electronics*, vol. 69, no. 1, pp. 151–159, Jan. 2022, doi: 10.1109/TIE.2021.3050349.

[17] Q. Sun, J. Wu, and C. Gan, "Optimized Direct Instantaneous Torque Control for SRMs with Efficiency Improvement," *IEEE Transactions on Industrial Electronics*, vol. 68, no. 3, pp. 2072–2082, Mar. 2021, doi: 10.1109/TIE.2020.2975481.

[18] S. Yao and W. Zhang, "A Simple Strategy for Parameters Identification of SRM Direct Instantaneous Torque Control," *IEEE Trans Power Electron*, vol. 33, no. 4, pp. 3622–3630, Apr. 2018, doi: 10.1109/TPEL.2017.2710137.

[19] H. Zeng, H. Chen, and J. Shi, "Direct instantaneous torque control with wide operating range for switched reluctance motors," *IET Electr Power Appl*, vol. 9, no. 9, pp. 578–585, Nov. 2015, doi: 10.1049/iet-epa.2015.0087.

[20] T. Husain, A. Elrayyah, Y. Sozer, and I. Husain, "Unified control for switched reluctance motors for wide speed operation," *IEEE Transactions on Industrial Electronics*, vol. 66, no. 5, pp. 3401–3411, May 2019, doi: 10.1109/TIE.2018.2849993.

[21] A. D. Cheok and Y. Fukuda, "A new torque and flux control method for switched reluctance motor drives," *IEEE Trans Power Electron*, vol. 17, no. 4, pp. 543–557, Jul. 2002, doi: 10.1109/TPEL.2002.800968.

[22] N. Yan, X. Cao, and Z. Deng, "Direct torque control for switched reluctance motor to obtain high torque-ampere ratio," *IEEE Transactions on Industrial Electronics*, vol. 66, no. 7, pp. 5144–5152, Jul. 2019, doi: 10.1109/TIE.2018.2870355.

[23] X. Ai-De, Z. Xianchao, H. Kunlun, and C. Yuzhao, "Torque-ripple reduction of SRM using optimised voltage vector in DTC," in *IET Electrical Systems in Transportation*, Mar. 2018, vol. 8, no. 1, pp. 35–43. doi: 10.1049/iet-est.2017.0090.

[24] J. H. Kim and R. Y. Kim, "Sensorless direct torque control using the inductance inflection point for a switched reluctance motor," *IEEE Transactions on Industrial Electronics*, vol. 65, no. 12, pp. 9336–9345, Dec. 2018, doi: 10.1109/TIE.2018.2821632.

[25] P. K. Reddy, D. Ronanki, and P. Perumal, "Efficiency improvement and torque ripple minimization of four-phase switched reluctance motor drive using new direct torque control strategy," *IET Electr Power Appl*, vol. 14, no. 1, pp. 52–61, Jan. 2020, doi: 10.1049/iet-epa.2019.0432.

[26] P. L. Chapman and S. D. Sudhoff, "Design and Precise Realization of Optimized Current Waveforms for an 8/6 Switched Reluctance Drive," 2002.

[27] R. Mikail, I. Husain, Y. Sozer, M. Islam, and T. Sebastian, "Torque Ripple Minimization of Switched Reluctance Machines through Current Profiling," 2013.

[28] S. Sayeed Mir, M. E. Elbuluk, S. Member, and I. Husain, "Torque-Ripple Minimization in Switched Reluctance Motors Using Adaptive Fuzzy Control," 1999.

[29] A. D. Cheok and N. Ertugrul, "Use of Fuzzy Logic for Modeling, Estimation, and Prediction in Switched Reluctance Motor Drives," 1999.

[30] C. Shang, D. Reay, and B. Williams, "Adapting CMAC Neural Networks with Constrained LMS Algorithm for Efficient Torque Ripple Reduction in Switched Reluctance Motors," 1999.

[31] X. D. Xue, K. W. E. Cheng, and S. L. Ho, “Optimization and evaluation of torque-sharing functions for torque ripple minimization in switched reluctance motor drives,” *IEEE Trans Power Electron*, vol. 24, no. 9, pp. 2076–2090, 2009, doi: 10.1109/TPEL.2009.2019581.

[32] F. Al-Amyal, L. al Quraan, and L. Szamel, “Torque Sharing Function Optimization for Extended Speed Range Control in Switched Reluctance Motor Drive,” pp. 000119–000124, 2021, doi: 10.1109/cando-epe51100.2020.9337792.

[33] J. Ye, B. Bilgin, and A. Emadi, “An Offline Torque Sharing Function for Torque Ripple Reduction in Switched Reluctance Motor Drives,” *IEEE Transactions on Energy Conversion*, vol. 30, no. 2, pp. 726–735, 2015, doi: 10.1109/TEC.2014.2383991.

[34] H. Li, B. Bilgin, and A. Emadi, “An Improved Torque Sharing Function for Torque Ripple Reduction in Switched Reluctance Machines,” *IEEE Trans Power Electron*, vol. 34, no. 2, pp. 1635–1644, 2019, doi: 10.1109/TPEL.2018.2835773.

[35] Y. Wei, M. Qishuang, Z. Poming, and G. Yangyang, “Torque ripple reduction in switched reluctance motor using a novel torque sharing function,” *AUS 2016 - 2016 IEEE/CSAA International Conference on Aircraft Utility Systems*, no. c, pp. 177–182, 2016, doi: 10.1109/AUS.2016.7748043.

[36] A. K. Rana and A. V. R. Teja, “A Mathematical Torque Ripple Minimization Technique Based on Nonlinear Modulating Factor for Switched Reluctance Motor Drives,” vol. 0046, no. c, 2021, doi: 10.1109/TIE.2021.3063871.

[37] Z. Xia, B. Bilgin, S. Nalakath, and A. Emadi, “A New Torque Sharing Function Method For Switched Reluctance Machines With Lower Current Tracking Error,” *IEEE Transactions on Industrial Electronics*, vol. 0046, no. c, 2020, doi: 10.1109/TIE.2020.3037987.

[38] X. D. Xue, K. W. E. Cheng, and S. L. Ho, “A control scheme of torque ripple minimization for SRM drives based on flux linkage controller and torque sharing function,” *2006 2nd International Conference on Power Electronics Systems and Applications, ICPESA*, no. 1, pp. 79–84, 2006, doi: 10.1109/PESA.2006.343074.

[39] T. H. Kim, D. H. Lee, and J. W. Ahn, “Advanced non-linear logic torque sharing function of SRM for torque ripple reduction,” *INTELEC, International Telecommunications Energy Conference (Proceedings)*, pp. 1–4, 2009, doi: 10.1109/INTLEC.2009.5351818.

[40] J. Ye, B. Bilgin, and A. Emadi, “An extended-speed low-ripple torque control of switched reluctance motor drives,” *IEEE Trans Power Electron*, vol. 30, no. 3, pp. 1457–1470, 2015, doi: 10.1109/TPEL.2014.2316272.

[41] R. Harikrishnan and F. M. Fernandez, “Improved online torque-sharing-function based low ripple torque control of switched reluctance motor drives,” *IEEE International Conference on Power Electronics, Drives and Energy Systems, PEDES 2016*, vol. 2016-Janua, pp. 1–6, 2017, doi: 10.1109/PEDES.2016.7914374.

[42] J. Ye and A. Emadi, “Power electronic converters for 12/8 switched reluctance motor drives: A comparative analysis,” *2014 IEEE Transportation Electrification Conference and Expo: Components, Systems, and Power Electronics - From Technology to Business and Public Policy, ITEC 2014*, 2014, doi: 10.1109/itec.2014.6861763.

[43] R. Krishnan, *Switched Reluctance Motor Drives: Modeling, Simulation, Analysis, Design, and Applications*. 2001. doi: 10.1201/9781420041644.

[44] G. Fang, F. Pinarello Scalcon, D. Xiao, R. Vieira, H. Grundling, and A. Emadi, “Advanced Control of Switched Reluctance Motors (SRMs): A Review on Current

Regulation, Torque Control and Vibration Suppression," *IEEE Open Journal of the Industrial Electronics Society*, vol. 2, no. March, pp. 280–301, 2021, doi: 10.1109/OJIES.2021.3076807.

[45] F. Peng, J. Ye, and A. Emadi, "A Digital PWM Current Controller for Switched," vol. 31, no. 10, pp. 7087–7098, 2016.

[46] I. Husain and M. Ehsani, "Torque Ripple Minimization in Switched Reluctance Motor Drives by PWM Current Control," *IEEE Trans Power Electron*, vol. 1, no. 1, pp. 104–107, 1996, doi: 10.1049/cp:20040267.

CURRICULUM VITAE

2015 - 2019	B.Sc., Electrical – Electronics Engineering, Osmangazi University, Eskişehir, Türkiye
2020 - 2023	M.Sc. Electrical and Computer Engineering, Abdullah Gül University, Kayseri, TURKEY
2020 - 2022	Graduate Research Assistant, Electrical - Electronics Engineering, Abdullah Gül University, Kayseri, TURKEY

SELECTED PUBLICATIONS AND PRESENTATIONS

J1) U. Genc, B. Tekgun, Instantaneous Torque Error Compensation Based Online Torque Sharing Function for Switched Reluctance Machines, in Review, Alexandria Engineering Journal, 2023.